



1 **Morphodynamic model of Lower Yellow River: flux or entrainment form** 2 **for sediment mass conservation?**

3 Chenge An¹, Andrew J. Moodie², Hongbo Ma², Xudong Fu¹, Yuanfeng Zhang³, Kensuke Naito⁴, Gary
4 Parker⁵

5 ¹Department of Hydraulic Engineering, State Key Laboratory of Hydrosience and Engineering, Tsinghua University,
6 Beijing, China.

7 ²Department of Earth, Environmental and Planetary Sciences, Rice University, Houston, TX, USA.

8 ³Yellow River Institute of Hydraulic Research, Zhengzhou, Henan, China.

9 ⁴Department of Civil and Environmental Engineering, Hydrosystems Laboratory, University of Illinois, Urbana-Champaign,
10 IL, USA.

11 ⁵Department of Civil and Environmental Engineering and Department of Geology, Hydrosystems Laboratory, University of
12 Illinois, Urbana-Champaign, IL, USA.

13 *Correspondence to:* Chenge An (anchenge08@163.com) and Xudong Fu (xdfu@tsinghua.edu.cn)

14 **Abstract.** Sediment mass conservation is a key factor that constrains river morphodynamic processes. In most models of river
15 morphodynamics, sediment mass conservation is described by the Exner equation, which may take various forms depending
16 on the problem in question. One of the most widely used forms of the Exner equation is the flux-based formulation, in which
17 the conservation of bed material is related to the streamwise gradient of the sediment transport rate. An alternate form of the
18 Exner equation, however, is the entrainment-based formulation, in which the conservation of bed material is related to the
19 difference between the entrainment rate of bed sediment into suspension and the deposition rate of suspended sediment onto
20 the bed. In the flux form, sediment transport is regarded to be in local equilibrium (i.e., sediment transport rate locally equals
21 sediment transport capacity). However, the entrainment form does not require this constraint: the sediment transport rate may
22 lag in space and time behind the changing flow conditions. In modeling the fine-grained Lower Yellow River, it is usual to
23 treat sediment conservation in terms of an entrainment (nonequilibrium) form rather than a flux (equilibrium) form, in
24 consideration of the condition that fine-grained sediment may be entrained at one place but deposited only at some distant
25 location downstream. However, the differences in prediction between the two formulations have not been comprehensively
26 studied to date. Here we study this problem by comparing the results of flux-based and entrainment-based morphodynamics
27 under conditions typical of the Lower Yellow River, but simplified for clarity of comparison. We used sediment transport
28 equations specifically designed for the Lower Yellow River. We find that in a treatment of a 200 km reach using a single
29 characteristic bed sediment size, there is little difference between the two forms since the corresponding adaptation length is
30 relatively small. However, a consideration of sediment mixtures shows that the two forms give very different patterns of grain
31 sorting: clear kinematic waves occur in the flux form but are diffused out in the entrainment form. Both numerical simulation



32 and mathematical analysis show that the morphodynamic processes predicted by the entrainment form are sensitive to sediment
33 fall velocity.

34 1. Introduction

35 Models of river morphodynamics often consist of three elements (Parker, 2004): (1) a treatment of flow hydraulics;
36 (2) a formulation relating some aspect of sediment transport to flow hydraulics; and (3) a description of sediment conservation.
37 In the case of unidirectional river flow, the Exner equation of sediment conservation has usually been described in terms of a
38 flux-based form in which temporal bed elevation change is related to the streamwise gradient of the sediment transport rate
39 $\partial q_s / \partial x$, where q_s is the total volumetric sediment transport rate per unit width and x is the streamwise coordinate (Exner, 1920;
40 Parker et al., 2004). This formulation is also referred to as the equilibrium formulation, since it considers sediment transport
41 to be at local equilibrium, i.e. q_s equals its sediment transport capacity q_{se} , regardless of the variation of flow conditions. Under
42 this assumption, sediment transport relations developed under equilibrium flow conditions (e.g., Meyer-Peter and Müller, 1948;
43 Engelund and Hansen, 1967; Brownlie, 1981) can be incorporated directly in such a formulation to calculate q_s , which is
44 related to one or more flow parameters such as bed shear stress.

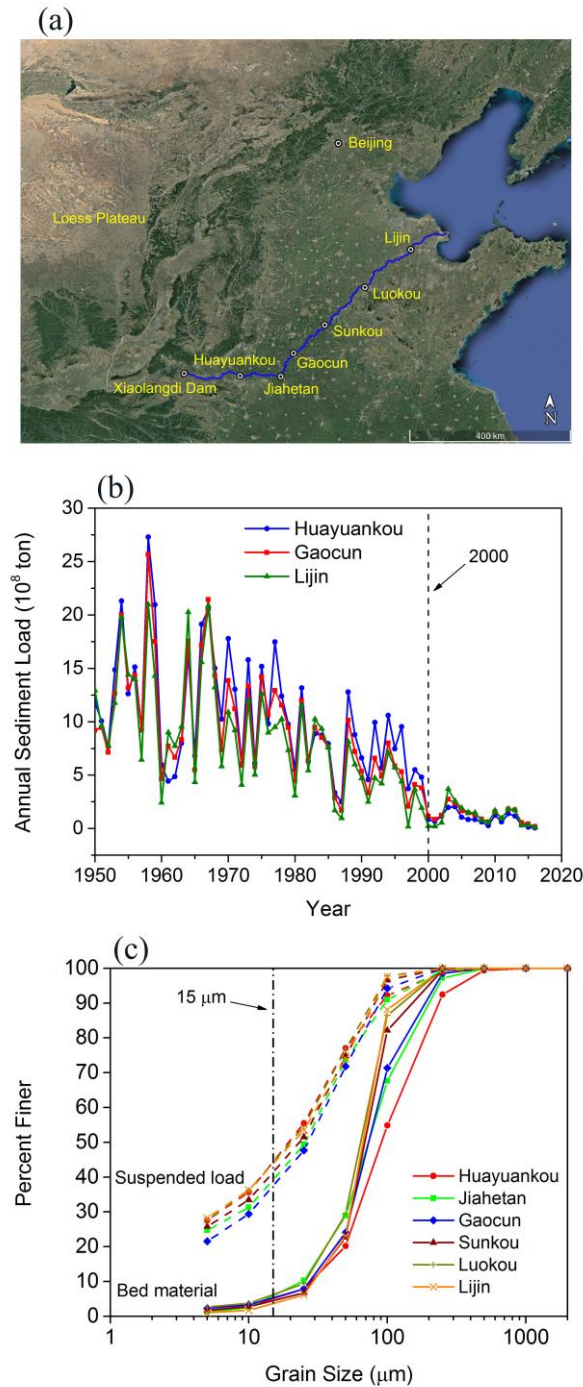
45 An alternate formulation, however, is available in terms of an entrainment-based form of the Exner equation, in which
46 bed elevation variation is related to the difference between the entrainment rate of bed sediment into suspension and the
47 deposition rate of suspended sediment on the bed (Parker, 2004). The basic idea of the entrainment formulation can be traced
48 back to Einstein (1937)'s pioneering work of bedload transport, and has been developed since then by numerous researchers
49 so as to treat either bedload or suspended load (Tsujiimoto, 1978; Armanini and Di Silvio, 1988; Parker et al., 2000; Wu and
50 Wang, 2008; Guan et al., 2015). Such a formulation differs from the flux formulation in that it is the rate of entrainment of bed
51 sediment, rather than the sediment transport rate itself, that is related to flow hydraulics. The difference between the local
52 entrainment rate from the bed and the local deposition rate onto the bed determines the rate of bed aggradation/degradation,
53 and concomitantly the rate of loss/gain of sediment in motion in the water column. Therefore, the sediment transport rate is no
54 longer assumed to be in an equilibrium transport state, but may exhibit lags in space and time after changing flow conditions.
55 The entrainment formulation is also referred to as the nonequilibrium formulation (Armanini and Di Silvio, 1988; Wu and
56 Wang, 2008; Zhang et al., 2013).

57 To describe the lag effects between sediment transport and flow conditions, the concept of an adaptation length/time
58 is widely applied. This length/time characterizes the distance/time for sediment transport to reach its equilibrium state (i.e.,
59 transport capacity). Using the concept of the adaptation length, the Exner equation can be recast into a first-order "reaction"
60 equation, in which the deformation term is related to the difference between the actual and equilibrium sediment transport
61 rates, as mediated by an adaptation length (which can also be recast as an adaptation time). (Armanini and Di Silvio, 1988;
62 Wu and Wang, 2008; Minh Duc and Rodi, 2008; El kadi Abderrezzak and Paquier, 2009). The adaptation length is thus an
63 important parameter for bed evolution under nonequilibrium sediment transport conditions, and various estimates have been



64 proposed. For suspended load, the adaptation length is typically calculated as a function of flow depth, flow velocity and
65 sediment fall velocity (Armanini and Di Silvio, 1988; Wu et al., 2004; Wu and Wang, 2008; Dorrell and Hogg, 2012; Zhang
66 et al., 2013). The adaptation length of bedload, on the other hand, has been related to a wide range of parameters, including
67 the sediment grain size (Armanini and Di Silvio, 1988), the saltation step length (Phillips and Sutherland, 1989), the dimensions
68 of particle diffusivity (Bohorquez and Ancey, 2016), the length of dunes (Wu et al., 2004), and the magnitude of a scour hole
69 formed downstream of an inerodible reach (Bell and Sutherland, 1983). For simplicity, the adaptation length can also be
70 specified as a calibration parameter in river morphodynamic models (El kadi Abderrezzak and Paquier, 2009; Zhang and Duan,
71 2011). Nonetheless, no comprehensive definition of adaptation length exists.

72 In this paper we apply the two forms of the Exner equation mentioned above to the Lower Yellow River (LYR) in
73 China. The LYR describes the river section between Tiexie and the river mouth, and has a total length of about 800 km. Figure
74 1(a) shows a sketch of the LYR along with 6 major gauging stations and the Xiaolangdi Dam, which is 26 km upstream of
75 Tiexie. The LYR has an exceptionally high sediment concentration (Ma et al., 2017), historically exporting more than 1 Gt of
76 sediment per year with only 49 billion tons of water, leading to a sediment concentration an order of magnitude higher than
77 most other large lowland rivers worldwide (Milliman and Meade, 1983; Ma et al., 2017; Naito et al., accepted subject to
78 revision). More recently, however, since the operation of Xiaolangdi Dam in 1999 the LYR has seen a substantial reduction
79 in its sediment load (Fig. 1(b)) because most of the sediment load is derived from the river reach upstream of the reservoir,
80 especially from the Loess Plateau (Wang et al., 2016; Naito et al., accepted subject to revision). Finally, the bed material of
81 the LYR is very fine, ranging as low as 15 μm . This is much finer than the conventional cutoff of washload (62.5 μm) employed
82 for sediment transport in most sand-bed rivers (National Research Council, 2007; Ma et al., 2017).



83
84 **Figure 1.** (a) Sketch of Lower Yellow River, showing 6 major gauging stations and the Xiaolangdi Dam; (b) Annual sediment
85 load of LYR measured at 3 gauging stations since 1950; (c) Grain size distributions of both bed material and suspended load
86 measured at 6 gauging stations of the LYR.



87
88 When modeling the high-concentration and fine-grained LYR, it is common to treat sediment conservation in terms
89 of an entrainment-based rather than a flux-based formulation. This is because many Chinese researchers view the entrainment
90 formulation as more physically based, and thus more likely to be capable of describing the behavior of fine-grained sediment,
91 which when entrained at one place may be deposited at some distant location downstream (Zhang et al., 2001; Ni et al., 2004;
92 Cao et al., 2006; He et al., 2012; Guo et al., 2008). However, the entrainment formulation is more computationally expensive
93 and more complex to implement. In so far as the differences in prediction between the two formulations do not appear to have
94 been studied in a systematic way, here we pose our central questions. Is the entrainment formulation really necessary when
95 modeling the LYR? Or more specifically, under what circumstances should a numerical modeler be impelled to implement the
96 entrainment formulation instead of the flux formulation for river morphodynamic modeling?

97 Here we study this problem by comparing the results of flux-based and entrainment-based morphodynamics under
98 conditions typical of the LYR. The organization of this paper is as follows. The numerical model is described in Section 2. In
99 Section 3, the model is implemented to predict the morphodynamics of the LYR. We find that the two forms of the Exner
100 equation give similar predictions in the case of uniform sediment, but show different sorting patterns in the case of sediment
101 mixtures. In Section 4, we conduct a mathematical analysis to explain the results in Section 3, and more specifically we quantify
102 the effects of varied sediment fall velocity in the simulations. Finally, we summarize our conclusions in Section 5.

103 2. Model formulation

104 In this paper, we present a one-dimensional morphodynamic model for the Lower Yellow River. The fully unsteady
105 Saint Venant Equations are implemented for the hydraulic calculation. As the main topic of this paper is to compare the flux
106 form and entrainment form of Exner equation, both the formulations of the Exner equation for sediment conservation are
107 implemented. For each formulation, we consider both the cases of uniform sediment (bed material characterized by a single
108 grain size) and sediment mixtures. Since the sediment is very fine in the LYR, the component of the load that is bedload is
109 likely negligible (e.g. Ma et al., 2017), so that we consider only the transport of suspended load. Considering the fact that most
110 well accepted sediment transport relations (e.g., the Engelund and Hansen, 1967 relation) underpredict the sediment transport
111 rate of the LYR by an order of magnitude or more (Ma et al., 2017), in our model we implement two recently developed
112 generalized versions of the Engelund-Hansen relation which are based on data from the LYR. These are the version of Ma et
113 al. (2017) for uniform sediment, and the version of Naito et al. (accepted subject to revision) for sediment mixtures. In cases
114 considering sediment mixtures, we also implement the method of Viparelli et al. (2010) to store and access bed stratigraphy
115 as the bed aggrades and degradates.

116 Some additional simplifications to the model facilitate comparison across the Exner formulation model runs. The
117 channel is simplified to be a constant-width rectangular channel, and bank (sidewall) effects and floodplain interactions are
118 not considered. The channel bed is assumed to be an infinitely deep supplier of erodible sediment with no exposed bedrock.



119 Finally, water and sediment are fed into the upstream boundary at a specified rate, and at the downstream end of the channel
120 we specify a fixed bed elevation along with a normal flow depth. These restrictions could be easily relaxed so as to incorporate
121 site-specific complexities of the Yellow River.

122 2.1 Flow hydraulics

123 Flow hydraulics in a rectangular channel is described by the following 1D Saint Venant equations, which consider
124 the fluid mass and momentum conservation,

$$125 \frac{1}{I_f} \frac{\partial h}{\partial t} + \frac{\partial q_w}{\partial x} = 0 \quad (1)$$

$$126 \frac{1}{I_f} \frac{\partial q_w}{\partial t} + \frac{\partial}{\partial x} \left(\frac{q_w^2}{h} + \frac{1}{2} gh^2 \right) = ghS - C_f u^2 \quad (2)$$

$$127 C_f = C_z^{-2} \quad (3)$$

128 where t is time, h is water depth, q_w is flow discharge per unit width, g is gravitational acceleration, S is bed slope, u is depth-
129 averaged flow velocity, C_f is dimensionless bed resistance coefficient, and C_z is the dimensionless Chezy resistance coefficient.
130 In our model, the fully unsteady 1D Saint Venant equations are solved using a Godunov type scheme with the HLL (Harten-
131 Lax-van Leer) approximate Riemann solver (Harten et al., 1983; Toro, 2001), which can effectively capture discontinuities in
132 unsteady and nonuniform open channel flows.

133 In this paper, the full flood hydrograph of the LYR is replaced by a flood intermittency factor I_f (Paola et al., 1992;
134 Parker, 2004). According to this definition, the river is assumed to be at low flow and not transporting significant amounts of
135 sediment for time fraction $1 - I_f$ and is in flood at constant discharge and active morphodynamically for time fraction I_f . In the
136 long term, the relation between the flood time scale t_f and the actual time scale t is $t_f = I_f t$. For all the governing equations in
137 this paper, the flood time scale is implemented by introducing I_f into each time derivative.

138 2.2 Flux form of the Exner equation

139 When dealing with uniform sediment, the flux form of the Exner equation can be written as,

$$140 \frac{1}{I_f} (1 - \lambda_p) \frac{\partial z_b}{\partial t} = - \frac{\partial q_s}{\partial x} \quad (4)$$



141 where λ_p is the porosity of the bed deposit, taken to be 0.4 in this paper and z_b is bed elevation. Sediment transport is regarded
 142 to be in a quasi-equilibrium state, so that the sediment transport rate per unit width q_s equals the equilibrium (capacity) sediment
 143 transport rate per unit width q_{se} .

144 When considering sediment mixtures, an active layer formulation (Hirano, 1971; Parker, 2004) is incorporated in the
 145 flux-based Exner equation, so that the evolution of both bed elevation and surface grain size distribution can be considered. In
 146 this formulation, the river bed is divided into a well-mixed upper active layer and a lower substrate with vertical stratigraphic
 147 variations. The upper active layer therefore represents the volume of sediment that interacts directly with suspended load
 148 transport, and also exchanges with the substrate as the bed aggrades and degrades. Discretizing the grain size distribution into
 149 n ranges, the mass conservation relation for each grain size range can be written as,

$$150 \quad \frac{1}{I_f} (1 - \lambda_p) \left[f_{ii} \frac{\partial}{\partial t} (z_b - L_a) + \frac{\partial}{\partial t} (F_i L_a) \right] = - \frac{\partial q_{si}}{\partial x} \quad (5)$$

151 where q_{si} is volumetric sediment transport rate per unit width of the i -th grain size range (taken to be equal to its equilibrium
 152 value q_{sei} in the flux formulation), F_i is the volumetric fraction of surface material in the i -th grain size range; f_{ii} is volumetric
 153 fraction of material in the i -th grain size range exchanged across the surface-substrate interface as the bed aggrades or degrades,
 154 and L_a is the thickness of active layer. For bedform-dominated sand-bed rivers, L_a is often related to the height of dunes so that
 155 the vertical sorting processes due to bedform migration can be considered (Blom et al., 2003). In this paper, a constant value
 156 of L_a is implemented in the simulation.

157 Summing Eq. (5) over all grain size ranges, one can find that the governing equation for bed elevation in case of
 158 sediment mixtures is the same as Eq. (4) upon replacing q_s with $q_{sT} = \sum q_{si}$, where q_{sT} denotes the total sediment transport rate
 159 per unit width summer over all size ranges. Reducing Eq. (5) with Eq. (4) we get,

$$160 \quad \frac{1}{I_f} (1 - \lambda_p) \left[L_a \frac{\partial F_i}{\partial t} + (F_i - f_{ii}) \frac{\partial L_a}{\partial t} \right] = f_{ii} \frac{\partial q_{sT}}{\partial x} - \frac{\partial q_{si}}{\partial x} \quad (6)$$

161 Therefore, in the flux formulation Eqs. (4) and (6) are implemented as governing equations for sediment mixtures,
 162 with Eq. (4) describing the evolution of bed elevation and Eq. (6) describing the evolution of surface grain size distribution.
 163 The exchange fractions f_{ii} between the active layer and the substrate are calculated using the following closure relation,

$$164 \quad f_{ii} = \begin{cases} f_i |_{z_b - L_a} & \frac{\partial z_b}{\partial t} < 0 \\ \alpha F_i + (1 - \alpha) p_{si} & \frac{\partial z_b}{\partial t} > 0 \end{cases} \quad (7)$$



165 That is, the substrate is transferred into the active layer during degradation, and a mixture of suspended load and active layer
166 material is transferred into substrate during aggradation. In Eq. (7), $f_{i|z_b-L_a}$ is the volumetric fraction of substrate material just
167 beneath the interface, $p_{si} = q_{si}/q_{sT}$ is the fraction of bed material load in the i -th grain size range, and α is a specified parameter
168 between 0 and 1. The formulation is adapted from Hoey and Ferguson (1994) and Toro-Escobar et al. (1996), who originally
169 used it for bedload. In this paper, a value of 0.5 is specified for α .

170 The method of Viparelli et al. (2010) is applied in our model to store substrate stratigraphy and provide information
171 for $f_{i|z_b-L_a}$ (i.e., the topmost sublayer in Viparelli et al., 2010). The reader can refer to the original reference of Viparelli et al.
172 (2010) for more details, or refer to An et al. (2017) for a concise description as how to implement this method in a
173 morphodynamic model.

174 2.3 Entrainment form of the Exner equation

175 The entrainment-based Exner equation for uniform sediment is,

$$176 \frac{1}{I_f} (1 - \lambda_p) \frac{\partial z_b}{\partial t} = -v_s (E - r_0 C) \quad (8)$$

177 In Eq. (8), v_s is the fall velocity of sediment particles; E is the dimensionless entrainment rate of sediment normalized by
178 sediment fall velocity; C is the depth-flux-averaged volume sediment concentration; and $r_0 = c_b/C$ is the recovery coefficient
179 of suspended load which denotes the ratio between the near-bed sediment concentration c_b and the flux-averaged sediment
180 concentration C . By definition, r_0 is related to the concentration profile of suspended load, and is expected to be no less than
181 unity in cases appropriate for a depth-averaged shallow-water treatment of flow and morphodynamics.

182 For sediment fall velocity v_s , we compare two widely used relations: the relation of Dietrich (1982), and the relation
183 of Ferguson and Church (2004). Results show that these two relations give almost the same fall velocity for bed material load
184 of the LYR, whose grain sizes typically fall in the range of 15 μm to 500 μm . Therefore, only the relation of Dietrich (1982) is
185 implemented in our simulations in this paper. Readers can refer to Appendix A for more details.

186 Since sediment transport is not necessarily in its equilibrium state in the entrainment formulation, we relate the
187 sediment entrainment rate, rather than the sediment transport rate, to the equilibrium sediment transport rate. Thus

$$188 E = r_0 \frac{q_{se}}{q_w} \quad (9)$$

189 For the depth-flux-averaged sediment concentration C , another equation is implemented describing the conservation of
190 suspended sediment in the water column,



$$191 \quad \frac{1}{I_f} \frac{\partial(hC)}{\partial t} + \frac{\partial(huC)}{\partial x} = v_s (E - r_0 C) \quad (10)$$

192 Note that sediment transport is at equilibrium when $E = r_0 C$. The sediment transport rate per unit width q_s obeys a continuity
 193 relation,

$$194 \quad q_s = huC \quad (11)$$

195 The entrainment-form Exner equation for sediment mixtures also uses the active layer formulation described in
 196 Section 2.2. Mass conservation of each grain size range can be written as,

$$197 \quad \frac{1}{I_f} (1 - \lambda_p) \left[f_{li} \frac{\partial}{\partial t} (z_b - L_a) + \frac{\partial}{\partial t} (F_i L_a) \right] = -v_{si} (E_i - r_{0i} C_i) \quad (12)$$

$$198 \quad E_i = r_{0i} \frac{q_{sei}}{q_w} \quad (13)$$

199 where the subscript i denotes the i -th size range of sediment grain size.

200 Summing Eq. (12) over all grain size ranges, we get the governing equation for bed elevation,

$$201 \quad \frac{1}{I_f} (1 - \lambda_p) \frac{\partial z_b}{\partial t} = - \sum_{j=1}^n v_{sj} (E_j - r_{0j} C_j) \quad (14)$$

202 Reducing Eq. (12) with Eq. (14) we get the governing equation for surface fraction F_i ,

$$203 \quad \frac{1}{I_f} (1 - \lambda_p) \left[L_a \frac{\partial F_i}{\partial t} + (F_i - f_{li}) \frac{\partial L_a}{\partial t} \right] = f_{li} \sum_{j=1}^n v_{sj} (E_j - r_{0j} C_j) - v_{si} (E_i - r_{0i} C_i) \quad (15)$$

204 The governing equation for the sediment concentration of each grain size C_i can be written as,

$$205 \quad \frac{1}{I_f} \frac{\partial(hC_i)}{\partial t} + \frac{\partial(huC_i)}{\partial x} = v_{si} (E_i - r_0 C_i) \quad (16)$$

206 and the sediment transport rate per unit width for the i -th size range q_{si} obeys the following continuity relation,

$$207 \quad q_{si} = huC_i \quad (17)$$

208 In the entrainment formulation, the closure relation for f_{li} is the same as that used in the flux formulation (i.e., Eq.
 209 (7)), and the substrate stratigraphy is also stored and accessed using the method of Viparelli et al. (2010).



210 2.4 Sediment transport relation

211 2.4.1 Uniform sediment

212 To close the Exner equations described in Sections 2.2 and 2.3, equations for equilibrium sediment transport rate q_{se}
213 (q_{sei}) are still needed. For the simulations using uniform sediment, we implement the generalized Engelund-Hansen relation
214 proposed by Ma et al. (2017). This equation is based on the data from LYR and can be written in the following dimensionless
215 form,

$$216 \quad q_s^* = \frac{\alpha_s}{C_f} (\tau^*)^{n_s} \quad (18)$$

217 where q_s^* is dimensionless sediment transport rate per unit width (i.e., the Einstein number), and τ^* is dimensionless shear
218 stress (i.e., the Shields number). They are defined as,

$$219 \quad q_s^* = \frac{q_{se}}{\sqrt{RgDD}} \quad (19)$$

$$220 \quad \tau^* = \frac{\tau_b}{\rho RgD} \quad (20)$$

$$221 \quad \tau_b = \rho C_f u^2 \quad (21)$$

222 where D is characteristic grain size of the bed sediment (here approximated as uniform); τ_b is bed shear stress; and R is
223 submerged specific gravity of sediment, defined as $(\rho_s - \rho) / \rho$, in which ρ_s is density of sediment, and ρ is density of water.
224 The sediment submerged specific gravity R is specified as 1.65 in this paper, which is an appropriate estimate for natural rivers,
225 and corresponds to quartz.

226 In the relation of Ma et al. (2017), the dimensionless coefficient $\alpha_s = 0.9$ and the dimensionless exponent $n_s = 1.68$.
227 These values are quite different from the original relation of Engelund and Hansen (1967), in which $\alpha_s = 0.05$ and $n_s = 2.5$.
228 Ma et al. (2017) demonstrated that such differences imply that the riverbed of the LYR is dominated by low-amplitude bedform
229 features (dunes) approaching upper-regime plane bed. According to this finding, form drag is then neglected in our modeling,
230 and all of the bed shear stress is used for sediment transport.

231 2.4.2 Sediment mixtures

232 We implement the relation of Naito et al. (accepted subject to revision) to calculate the equilibrium sediment transport
233 rate of size mixtures. Using field data from the LYR, Naito et al. (accepted subject to revision) extended the Engelund and



234 Hansen (1967) relation to a surface-based grain-size specific form, in which the suspended load transport rate of the i -th size
 235 range is tied to the availability of this size range on bed surface:

$$236 \quad q_{sei} = \frac{N_i^* F_i u_*^3}{RgC_f} \quad (22)$$

237 where N_i^* is the dimensionless sediment transport rate in the i -th size range, and u_* is shear velocity calculated from the bed
 238 shear stress τ_b :

$$239 \quad u_* = \sqrt{\frac{\tau_b}{\rho}} \quad (23)$$

240 The transport relation itself takes the form,

$$241 \quad N_i^* = A_i \left(\tau_g^* \frac{D_{sg}}{D_i} \right)^{B_i} \quad (24)$$

242 in which D_i is the characteristic grain size for sediment in the i -th size range, D_{sg} is the geometric mean grain size in the active
 243 layer, and τ_g^* is the dimensionless bed shear stress associated with D_{sg} . The parameters τ_g^* , coefficient A_i , and exponent B_i are
 244 calculated as,

$$245 \quad \tau_g^* = \frac{\tau_b}{\rho RgD_{sg}} \quad (25)$$

$$246 \quad A_i = 0.46 \left(\frac{D_i}{D_{sg}} \right)^{-0.84} \quad (26)$$

$$247 \quad B_i = 0.35 \left(\frac{D_i}{D_{sg}} \right)^{-1.16} \quad (27)$$

248 The forms of Eqs. (26) and (27) indicate that the hiding effects between coarse and fine sediment play a role in this
 249 sediment transport relation.



250 3. Numerical modeling of the LYR using the two forms of Exner equation

251 In this section, we conduct numerical simulations using both the flux form and the entrainment form of the Exner
252 equation, with the aim to study under what circumstances the two forms give different predictions. Numerical simulations are
253 conducted in the setting of the LYR. We specify a 200 km long channel reach for our simulations, along with a constant
254 channel width of 300 m and an initial longitudinal slope of 0.0001. Bed porosity λ_p is specified as 0.4. Based on field
255 measurements of the LYR available to us, we implemented a dimensionless Chezy resistance coefficient C_z of 30, which
256 corresponds to a dimensionless bed resistance coefficient C_f of 0.0011. For the entrainment form of Exner equation, we specify
257 the ratio of near bed sediment concentration to flux-averaged sediment concentration r_0 (r_{0i}) = 1. Such a value of r_0 (r_{0i})
258 corresponds to a vertically uniform profile of sediment concentration, and will thus give a maximum difference between the
259 prediction of entrainment form and the prediction of the flux form. More discussion about the effects of r_0 will be presented
260 in Section 4.3.

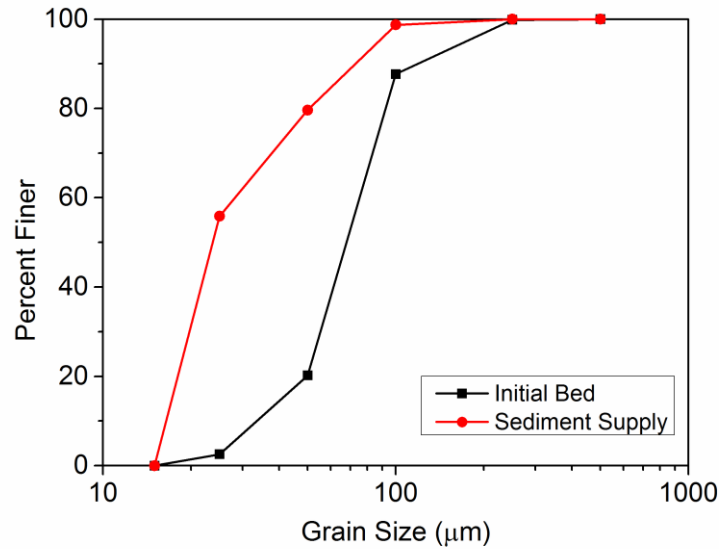
261 A constant flow discharge of 2000 m³/s (corresponding to a flow discharge per unit width q_w of 6.67 m²/s) is
262 introduced at the inlet of the channel with the flood intermittency factor I_f estimated as 0.14 (Naito et al., accepted subject to
263 revision). The downstream end is specified far from the river mouth to neglect the effects of backwater. Therefore, the bed
264 elevation is held constant and the water depth is specified as the normal flow depth at the downstream end of the calculational
265 domain. The above flow discharge per unit width q_w combined with the bed slope S as well as the bed resistance coefficient C_f
266 leads to a normal flow depth of 3.69 m. In our simulation, we use the height of bedforms in the LYR to determine the thickness
267 of the active layer (Blom et al., 2003). According to the field survey of Ma et al. (2017), the characteristic height of bedforms
268 in the LYR is about 20% of the normal flow depth, which can fall in the range suggested by the data analysis of Bradley and
269 Venditti (2017). This eventually leads to an estimate of active layer thickness of $L_a = 0.738$ m.

270 Two cases are considered here. In the first case, the sediment grain size distribution of LYR is simplified to a uniform
271 grain size of 65 μm . This is based on the measured grain size distribution of bed material at the Lijin gauging station, which
272 has a median grain size of $D_{50} = 66.6$ μm and a geometric mean grain size of $D_g = 65.5$ μm , as shown in Fig. 1(c). In the second
273 case, we consider the effects of sediment mixtures. The grain size distribution of the initial bed is based on the bed material at
274 the Lijin gauging station as shown in Fig. 1(c), but we renormalize the measured grain size distribution with a cutoff for
275 washload at 15 μm as suggested by Ma et al. (2017). The renormalized grain size distribution for the initial bed as implemented
276 in the case of sediment mixtures is shown in Fig. 2. In both the two cases, simulations start with an equilibrium state where
277 sediment supply rate = sediment transport rate = equilibrium sediment transport rate, so that the initial state of the channel is
278 in equilibrium. Then we cut the sediment supply rate (of each size range) to only 10% of the equilibrium sediment transport
279 rate and keep this sediment supply rate. This is to mimic the reduction of sediment load in the LYR in recent years, as shown
280 in Fig. 1(b). The grain size distribution of sediment supply in the case of sediment mixtures is shown in Fig. 2.

281 The 200 km channel reach is discretized into 401 cells, with cell size Δx of 500 m. In the case of uniform sediment,
282 we specify a time step for morphologic calculation $\Delta t_m = 10^{-4}$ year and a time step for hydraulic calculation $\Delta t_h = 10^{-6}$ year. In



283 the case of sediment mixtures, we specify a time step for morphologic calculation $\Delta t_m = 10^{-5}$ year, and a time step for hydraulic
 284 calculation $\Delta t_h = 10^{-6}$ year. Computational conditions are briefly summarized in Table 1. The computational conditions we
 285 implement are much simpler than the rather complicated conditions of the actual LYR. But it should be noted that the aim of
 286 this paper is not to reproduce specific aspects of the morphodynamic processes of LYR, but to compare the flux form and
 287 entrainment form of Exner equation in the context of conditions typical of LYR.



288 **Figure 2.** Grain size distributions of both the initial bed and the sediment supply in the case of sediment mixtures. The grain
 289 size distribution of the initial bed is renormalized based on the field data at the Lijin gauging station. The grain size distribution
 290 of the sediment supply equals to the grain size distribution of bed material load at equilibrium. Washload sizes have been
 291 removed from both distributions.
 292

293 **Table 1.** Summary of computational conditions for numerical modeling of the LYR.

Parameter	Value
Channel length L	200 km
Channel width B	300 m
Initial slope S_I	0.0001
Dimensionless Chezy resistance coefficient C_z	30
Flow discharge per unit width q_w	6.67 m ² /s
Flood intermittency factor I_f	0.14
ratio of near bed concentration to average concentration r_0 (r_{0i})	1
Characteristic grain size in the case of uniform sediment	65 μm
Submerged specific gravity of sediment R	1.65
Porosity of bed deposits λ_p	0.4

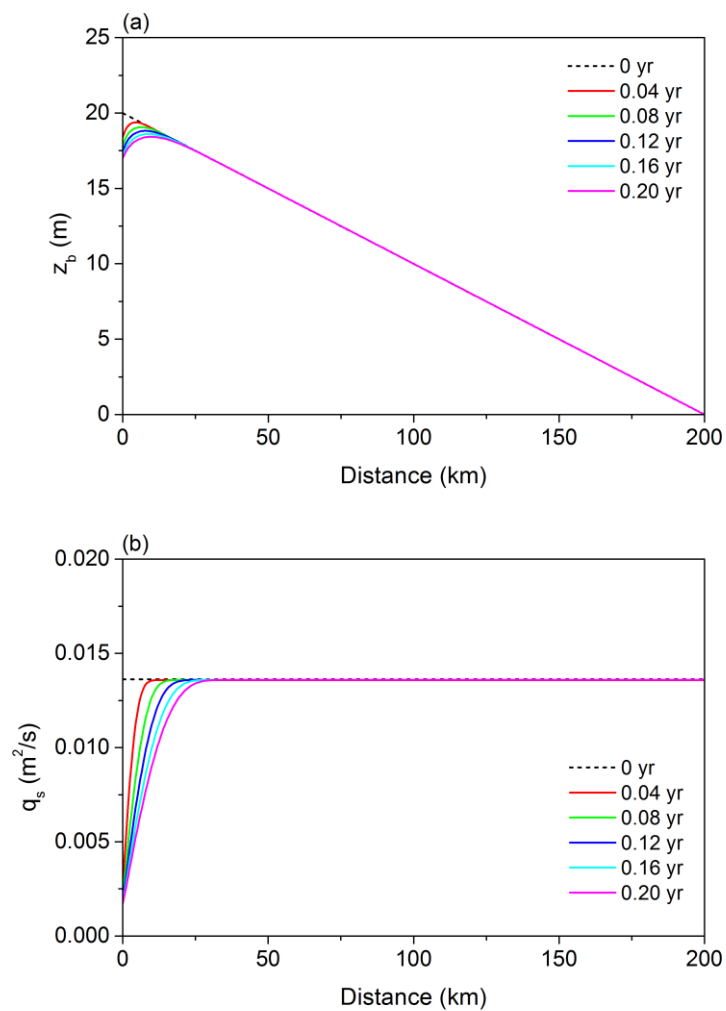


294

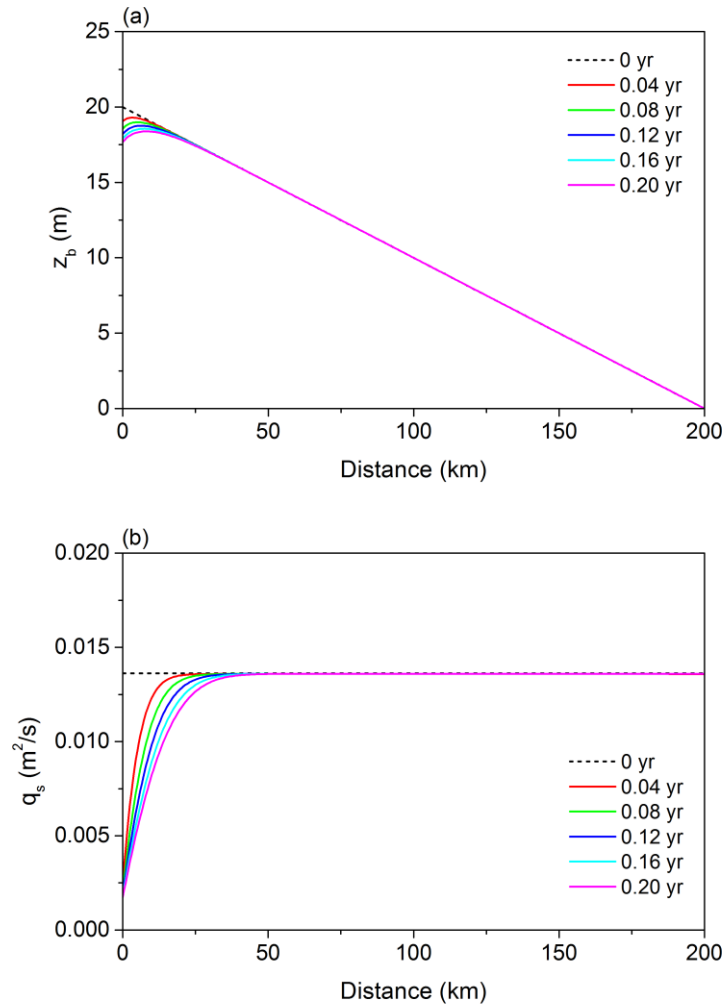
295 3.1 Case of uniform sediment

296 In this case, we implement a uniform grain size of 65 μm for both the bed material and sediment supply. Such a grain
297 size is nearly equal to the observed median grain size (or geometric mean grain size) of bed material at Lijin gauging station.
298 The relation of Ma et al. (2017) is implemented to calculate the transport rate of bed material suspended load. This relation
299 provides an equilibrium sediment transport rate per unit width q_{se} of 0.0136 m^2/s under the given flow discharge, bed slope
300 and sediment grain size. With a flood intermittency factor I_f of 0.14, this further gives a mean annual bed material load of 47.8
301 Mt/a. Adding in washload according to the estimate of Naito et al. (accepted subject to revision), total mean annual load is
302 86.9 Mt/a, a value that is of the same order of magnitude as averages over the period 2000-2016 (89-126 Mt/a depending on
303 site), i.e. since the operation of Xiaolangdi Dam in 1999 (Fig. 1(b)). The sediment supply rate q_{sf} we specify at the upstream
304 end of the channel is only 10% of the equilibrium sediment transport rate (i.e. sediment supply rate is cut by 90% from the
305 equilibrium state), such that $q_{sf} = 0.00136 \text{ m}^2/\text{s}$.

306 Figure 3 shows the modeling results using the flux form of the Exner equation. As we can see in the figure, the bed
307 degrades and the sediment load decreases in response to the cutoff of sediment supply. Such adjustments start from the
308 upstream end of the channel and gradually migrate downstream. Figure 4 shows the modeling results using the entrainment
309 form of Exner equation. A comparison between Fig. 4 and Fig. 3 shows that the entrainment form and the flux form give very
310 similar predictions in this case. The entrainment form provides a somewhat slower degradation and a more diffusive sediment
311 load reduction. Such more diffusive predictions of sediment load variation can be ascribed to the concept of nonequilibrium
312 transport that is embedded in the entrainment form. This issue will be studied analytically in Section 4. Here we present the
313 results of only 0.2 year after the cutoff of sediment supply, since the differences between the predictions of the two forms tend
314 to be the most evident shortly after the disruption but gradually diminish as the river approaches the new equilibrium (El kadi
315 Abderrezzak and Paquier, 2009). Modeling results over a longer time scale will be discussed in Section 4.3.



316
317 **Figure 3.** 0.2 year results for the case of uniform sediment using the flux form of Exner equation: time variation of (a) bed
318 elevation z_b and (b) sediment load per unit width q_s of the LYR in response to the cutoff of sediment supply.



319
 320 **Figure 4.** 0.2 year results for the case of uniform sediment using the entrainment form of Exner equation: time variation of (a)
 321 bed elevation z_b and (b) sediment load per unit width q_s of the LYR in response to the cutoff of sediment supply.

322 To further quantify the differences between the predictions of the two forms, we propose the following normalized
 323 parameter,

$$324 \quad \delta(y) = \left| \frac{y_E - y_F}{y_F} \right| \times 100\% \quad (28)$$

325 where y denotes an arbitrary variable calculated by the morphodynamic model, and subscripts F and E denote results using the
 326 flux form and the entrainment form respectively. Therefore, $\delta(y)$ denotes the difference between the prediction the two forms
 327 y_F and y_E normalized by the prediction of the flux form y_F .

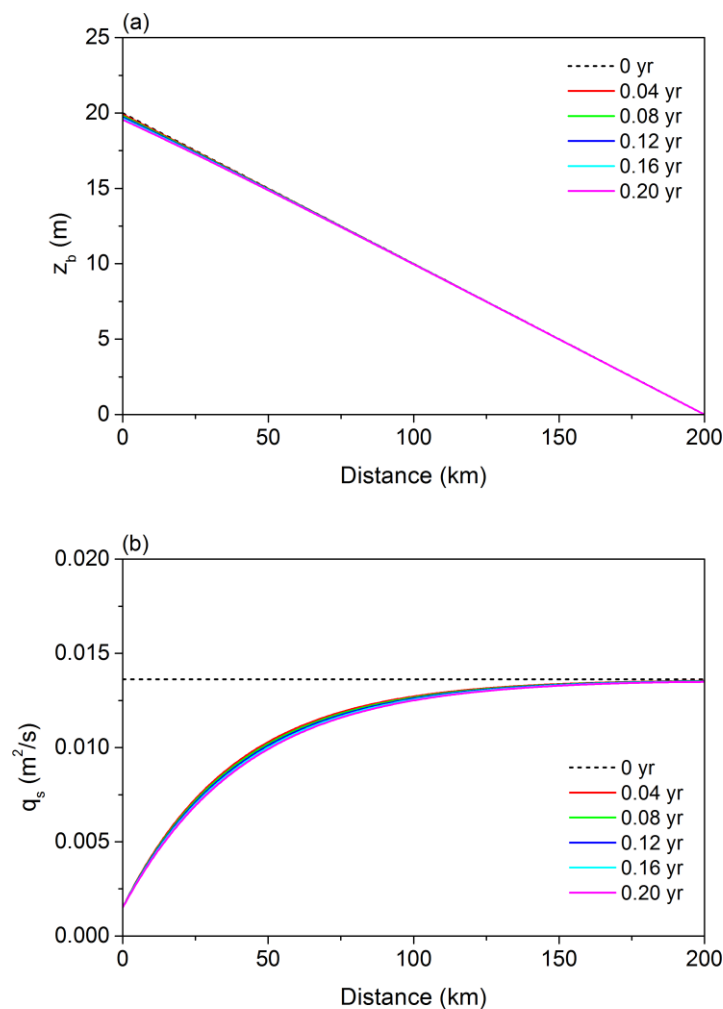


328 Table 2 gives a summary of the maximum values of δ along the channel at different times in the case of uniform
 329 sediment. The values of δ for both z_b and q_s are presented. As we can see from the table, the maximum value of $\delta(z_b)$ along the
 330 calculational domain keeps within 4% in the first 0.2 year after the cutoff of sediment supply. This indicates that the flux form
 331 and the entrainment form can indeed give almost the same prediction in terms of bed elevation in this case. But in the case of
 332 the sediment load per unit width q_s , the maximum value of $\delta(q_s)$ can be as high as 20%, indicating that even though the two
 333 forms give qualitatively similar patterns of evolution in terms of sediment load as shown in Figs. 3 and 4, the quantitative
 334 difference can be clearly evident due to the more diffusive nature of the predictions of the entrainment form. The value of $\delta(q_s)$
 335 is largest at the beginning of the simulation, and then gradually reduces with time.

336 **Table 2.** Quantification of the difference between predictions of the flux form and the entrainment form in the case of uniform
 337 sediment. The maximum values of $\delta(z_b)$ and $\delta(q_s)$ in the calculational domain are presented every 0.04 year.

		0.04 yr	0.08 yr	0.12 yr	0.16 yr	0.20 yr
original v_s	$\delta(z_b)$	3.66 %	3.91 %	3.93 %	3.88 %	3.81 %
	$\delta(q_s)$	20.48 %	15.11 %	12.31 %	10.48 %	9.17 %
v_s multiplied by 0.05	$\delta(z_b)$	8.23 %	10.94 %	12.66 %	13.92 %	14.91 %
	$\delta(q_s)$	74.83 %	68.14 %	63.04 %	58.89 %	55.41 %

338
 339 The above results show that the flux form and the entrainment form can provide similar predictions of LYR when the
 340 bed sediment grain size distribution is simplified to a uniform value of 65 μm . To understand under what conditions the two
 341 forms will lead to more different results, we conduct an idealized run using the entrainment form in which the sediment fall
 342 velocity v_s is arbitrarily multiplied by a factor of 0.05. That is to say, we keep the sediment grain size at 65 μm in the
 343 computation of the Shields number, but let the sediment fall velocity in Eqs. (8) and (10) equal only 1/20 of the value calculated
 344 by the relation of Dietrich (1982) from this grain size. With a much smaller, and indeed intentionally unrealistic sediment fall
 345 velocity, the entrainment form predicts very different results as shown in Fig. 5. The adjustments of the sediment load become
 346 even more diffusive in space: it almost takes the entire 200 km reach for the sediment load to adjust from the upstream
 347 disruption to the equilibrium transport rate. Meanwhile, there is barely any bed degradation at the upstream end after 0.2 year,
 348 in correspondence with the fact that the spatial gradient of q_s becomes quite small. In Table 2 we also exhibit the δ values for
 349 this idealized run. It is no surprise that both $\delta(z_b)$ and $\delta(q_s)$ are high, as the entrainment form and flux form predict very different
 350 patterns with such an arbitrarily reduced sediment fall velocity.



351
352 **Figure 5.** 0.2 year results for the case of uniform sediment using the entrainment form of Exner equation: time variation of (a)
353 bed elevation z_b and (b) sediment load per unit width q_s of the LYR in response to the cutoff of sediment supply. Sediment fall
354 velocity v_s is arbitrarily multiplied by a factor of 0.05 while holding bed grain size constant in this run.

355 3.2 Case of sediment mixtures

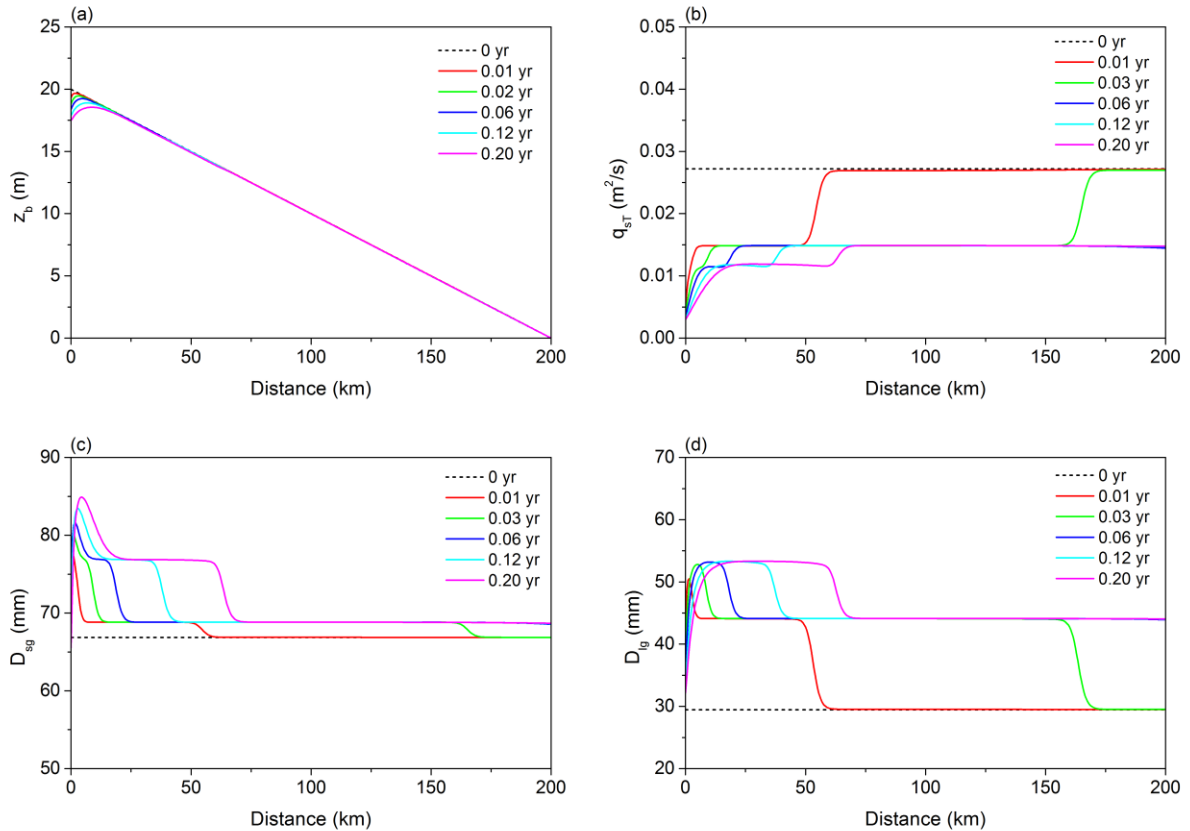
356 In this section we consider the morphodynamics of sediment mixtures rather than the case of a uniform bed grain size
357 implemented in section 3.1. The grain size distribution of the initial bed is based on field data at the Lijin gauging station, and
358 is shown in Fig. 2. Using the sediment transport relation of Naito et al. (accepted subject to revision) for mixtures, such a grain
359 size distribution combined with the given bed slope and flow discharge leads to a total equilibrium sediment transport rate per
360 unit width q_{seT} of $0.0272 m^2/s$. With a flood intermittency factor I_f of 0.14, this further gives a mean annual bed material load
361 of 95.5 Mt/a. Adding in washload according to the estimate of Naito et al. (accepted subject to revision), total mean annual



362 load 173.7 Mt/a, a value that is of the same order of magnitude as averages over the period 2000-2016 (89-126 Mt/a depending
363 on site), i.e. since the operation of Xiaolangdi Dam in 1999 (Fig. 1(b)). The sediment supply rate of each grain size range is
364 set at 10% of its equilibrium sediment transport rate. This results in a total sediment supply rate of $q_{sf} = 0.00272 \text{ m}^2/\text{s}$, and a
365 grain size distribution of the sediment supply (shown in Fig. 2) that is identical to the grain size distribution of the equilibrium
366 sediment load. Again we exhibit simulation results for only 0.2 year here, a value that is enough to show the differences
367 between the two forms, flux and entrainment, as applied to mixtures. Modeling results over a longer time scale are presented
368 in Section 4.3.

369 Figure 6 shows the simulation results using the flux form of the Exner equation. As a result of the reduced sediment
370 supply at the inlet, bed degradation occurs first at the upstream end and then gradually migrates downstream. The total sediment
371 transport rate per unit width q_{sT} also reduces as a response to the cutoff of sediment supply. More specifically, the evolution
372 of q_{sT} shows marked evidence of advection, with at least two kinematic waves being observed within 0.2 year. As shown in
373 Fig. 6(b), the fastest kinematic wave migrates beyond the 200 km reach within 0.06 year, and the second fastest kinematic
374 wave migrates for a distance of about 60 km in 0.2 year. Figures 6(c) and 6(d) show the results for the surface geometric mean
375 grain size D_{sg} and geometric mean grain size of suspended load D_{lg} respectively. As can be seen therein, both the bed surface
376 and the suspended load coarsen as a result of the cutoff of sediment supply. Such coarsening is not evident near the upstream
377 end, possibly due to the inverse slope visible in Fig. 6(a). Similarly to the variation of q_{sT} , the patterns of time variation of both
378 D_{sg} and D_{lg} also exhibit very clear kinematic waves, with migration rates about the same as those of q_{sT} .

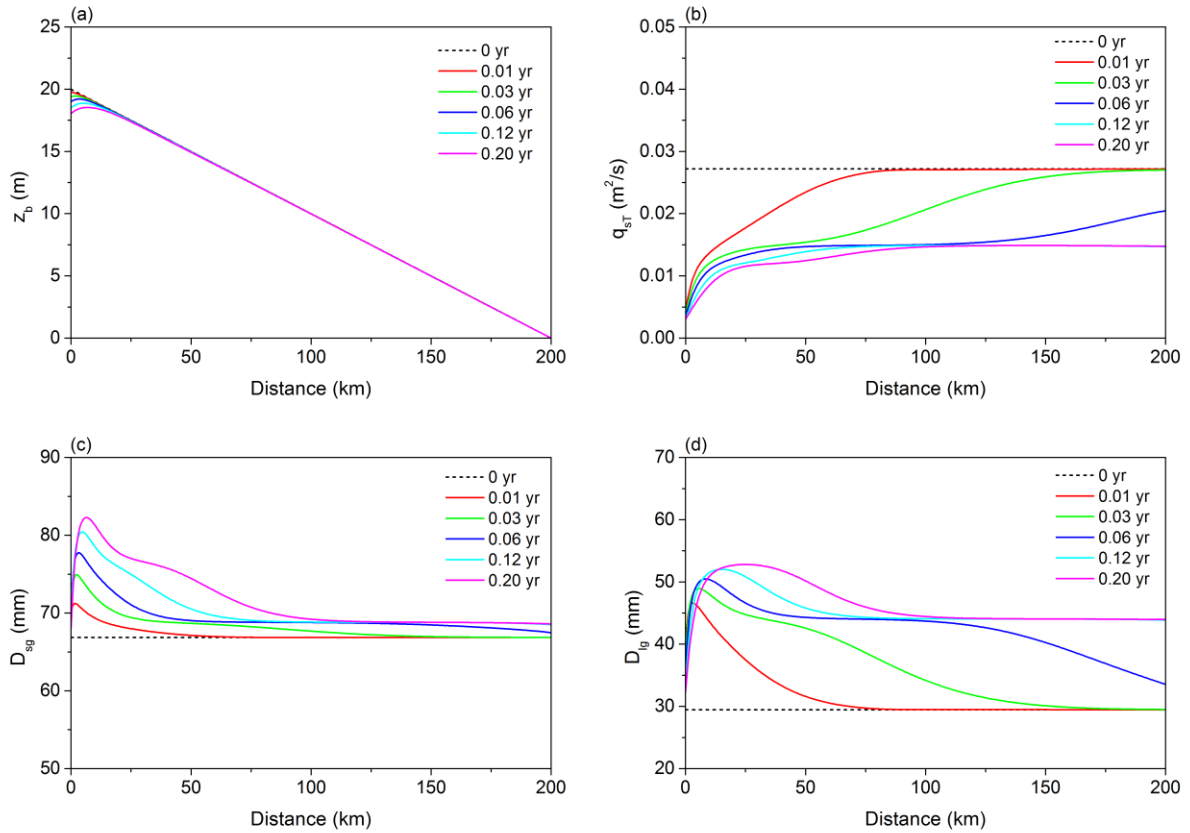
379



380 **Figure 6.** 0.2 year results for the case of sediment mixtures using the flux form of Exner equation: time variation of (a) bed
 381 elevation z_b , (b) total sediment load q_{ST} , (c) surface geometric mean grain size D_{sg} and (d) geometric mean grain size of sediment
 382 load of the LYR in response to the cutoff of sediment supply.
 383

384 Figure 7 shows the simulation results obtained using the entrainment form of the Exner equation. In general, the
 385 patterns of variation predicted by the entrainment form have similar trends and magnitudes to those predicted by the flux form:
 386 the bed degrades near the upstream end, the suspended load transport rate reduces in time, and both the bed surface and the
 387 suspended load coarsen as a result of the cutoff of sediment supply. But the results based on the two forms exhibit very evident
 388 differences when multiple grain sizes are included. That is, the results predicted by the entrainment form are sufficiently
 389 diffusive so that the variations of q_{ST} , D_{sg} , and D_{lg} (Figs. 7(b), 7(c) and 7(d)) do not show the advective character seen in Fig.
 390 6. No clear kinematic waves can be observed in Fig. 7. Table 3 gives a summary of the values of δ in the case of sediment
 391 mixtures. The prediction of bed elevation is not affected much when multiple grain sizes are considered, with $\delta(z_b)$ being no
 392 more than 3.5% within 0.2 year. The δ values of q_{ST} , D_{sg} , and D_{lg} are, however, relatively large since the two forms predict
 393 quite different patterns of variations, as shown in Fig. 6 and Fig. 7.

394



395
 396 **Figure 7.** 0.2 year results for the case of sediment mixtures using the entrainment form of Exner equation: time variation of
 397 (a) bed elevation z_b , (b) total sediment load q_{sT} , (c) surface geometric mean grain size D_{sg} and (d) geometric mean grain size
 398 of sediment load of the LYR in response to the cutoff of sediment supply.

399 **Table 3.** Quantification of the difference between predictions of the flux form and the entrainment form in the case of sediment
 400 mixtures. The maximum values of δ in the calculational domain are presented at different times.

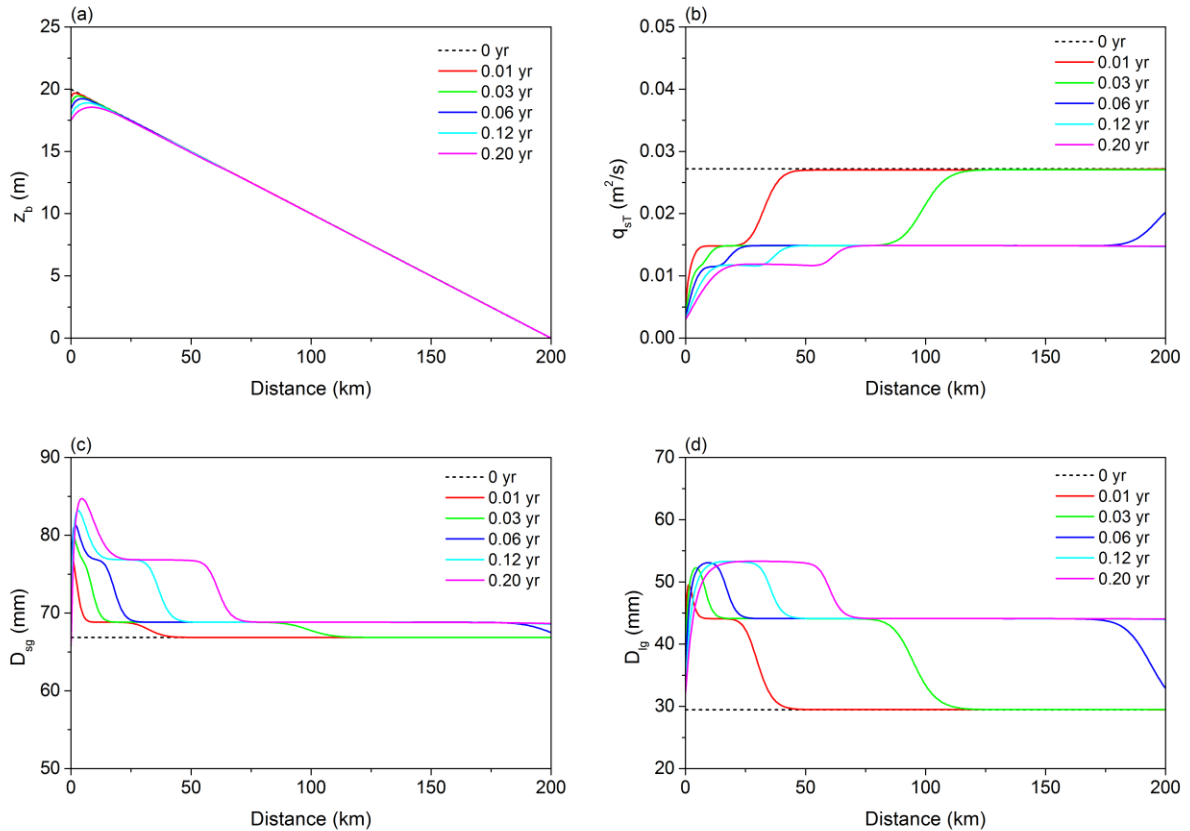
		0.01 yr	0.03 yr	0.06 yr	0.12 yr	0.20 yr
original v_s	$\delta(z_b)$	2.31 %	3.15 %	3.44 %	3.44 %	3.24 %
	$\delta(q_{sT})$	54.66 %	76.11 %	41.13 %	10.45 %	11.77 %
	$\delta(D_{sg})$	10.07 %	8.60 %	7.18 %	6.02 %	5.40 %
	$\delta(D_{lg})$	27.10 %	31.87 %	23.67 %	7.16 %	7.68 %
v_s multiplied by 20	$\delta(z_b)$	0.27 %	0.40 %	3.83 %	0.26 %	0.21 %
	$\delta(q_{sT})$	81.12 %	82.26 %	39.65 %	7.15 %	9.28 %
	$\delta(D_{sg})$	2.81 %	2.84 %	1.96 %	2.65 %	3.41 %
	$\delta(D_{lg})$	32.78 %	33.11 %	25.13 %	4.77 %	6.02 %

401



402 The results shown in Fig. 8 have also been calculated using the entrainment form of the Exner equation, but here the
403 sediment fall velocities v_{si} used in Eqs. (14)-(16) are arbitrarily multiplied by a factor of 20. That is, we still apply the grain
404 size distribution in Fig. 2, but the sediment fall velocities implemented in the simulation are 20 times the corresponding fall
405 velocities calculated by the relation of Dietrich (1982). In the case of uniform sediment in Section 3.1, we arbitrarily reduce
406 the sediment fall velocity to force a difference between the predictions from the entrainment form and those from the flux form.
407 Here we arbitrarily increase the sediment fall velocity with the aim of determining under what conditions the sorting patterns
408 predicted by the two forms converge. As we can see in Fig. 8, with such a larger and intentionally unrealistic sediment fall
409 velocity, the general trend of variations predicted by the entrainment form does not change, but the results show a notably less
410 diffusive pattern. The variations of q_{sT} , D_{sg} , and D_{lg} show more advection compared with Fig. 7, and at least two kinematic
411 waves appear within 0.2 year. It should be noted that even though these kinematic waves appear after we arbitrarily increase
412 the sediment fall velocity, they are more diffusive than those obtained from the flux formulation and also migrate with a slower
413 celerity as compared with those predicted by the flux form, especially for the fastest kinematic wave in the modeling results.

414 Table 3 summarizes the δ values for this run. The values of $\delta(z_b)$ become smaller with arbitrarily increased sediment
415 fall velocities except for $t = 0.06$ year. A relatively large value of $\delta(z_b)$ at $t = 0.06$ year occurs near the downstream end of the
416 channel, where the entrainment form predicts some slight degradation. Also, $\delta(q_{sT})$ is quite large at $t = 0.01$ year and 0.03 year,
417 even though the results for the case of increased fall velocities become qualitatively more similar to the prediction of the flux
418 form. This is because the flux form and the entrainment form with arbitrarily increased sediment fall velocities predict different
419 celerities for the fastest kinematic wave. The error $\delta(q_{sT})$ becomes smaller from $t = 0.06$ year as the fastest kinematic wave
420 migrates beyond the channel reach. The error $\delta(D_{lg})$ behaves similarly to $\delta(q_{sT})$, with $\delta(D_{lg})$ being quite large at $t = 0.01$ year
421 and 0.03 year near the fastest kinematic wave, but gradually becoming smaller as time passes. The error $\delta(D_{sg})$ stays low within
422 the whole 0.2 year period, possibly because the fastest kinematic wave of D_{sg} has a small magnitude, as shown in Fig. 8(c).



423
 424 **Figure 8.** 0.2 year results for the case of sediment mixtures using the entrainment form of Exner equation: time variation of
 425 (a) bed elevation z_b , (b) total sediment load q_{sT} , (c) surface geometric mean grain size D_{sg} and (d) geometric mean grain size
 426 of sediment load of the LYR in response to the cutoff of sediment supply. Sediment fall velocities v_{si} are arbitrarily multiplied
 427 by a factor of 20 in this run while keeping the grain sizes invariant.

428 **4. Discussion**

429 **4.1 Adjustment of sediment load and the adaptation length**

430 In Section 3.1, our simulation shows that in the case of uniform sediment, the flux form and the entrainment form of
 431 the Exner equation give very similar predictions for a given sediment size of 65 μm . However, if we arbitrarily reduce the
 432 sediment fall velocity by a multiplicative factor of 0.05, the prediction given by the entrainment form will become much more
 433 diffusive, in terms of both z_b and q_s . The diffusive nature of the entrainment form as well as the important role played by the
 434 sediment fall velocity can be explained in terms of the governing equation.

435 In the entrainment form, the equation governing suspended sediment concentration is,



$$436 \quad \frac{1}{I_f} \frac{\partial(hC)}{\partial t} + \frac{\partial(huC)}{\partial x} = v_s (E - r_0 C) \quad (29)$$

437 i.e. the same as Eq. (10). The sediment transport rate per unit width $q_s = huC = q_w C$, and the dimensionless entrainment rate
 438 $E = r_0 q_{se} / q_w$. If we consider only the adjustment of sediment concentration in space and neglect the temporal derivative in Eq.
 439 (29), we get

$$440 \quad \frac{\partial q_s}{\partial x} = v_s (E - r_0 C) = \frac{1}{L_{ad}} (q_{se} - q_s) \quad (30)$$

$$441 \quad L_{ad} = \frac{q_w}{v_s r_0} \quad (31)$$

442 where L_{ad} can be identified as the adaptation length for suspended sediment to reach equilibrium. This definition of adaptation
 443 length is similar to those in Wu and Wang (2008), and Ganti et al. (2014).

444 If we consider the spatial adjustment of sediment load shortly after the cutoff of sediment supply, we can further
 445 neglect the nonuniformity of the capacity (equilibrium) transport rate q_{se} along the channel, and Eq. (30) can be solved with a
 446 given upstream boundary condition. That is, with the boundary condition

$$447 \quad q_s \Big|_{x=0} = q_{sf} \quad (32)$$

448 Eq. (30) can be solved to yield

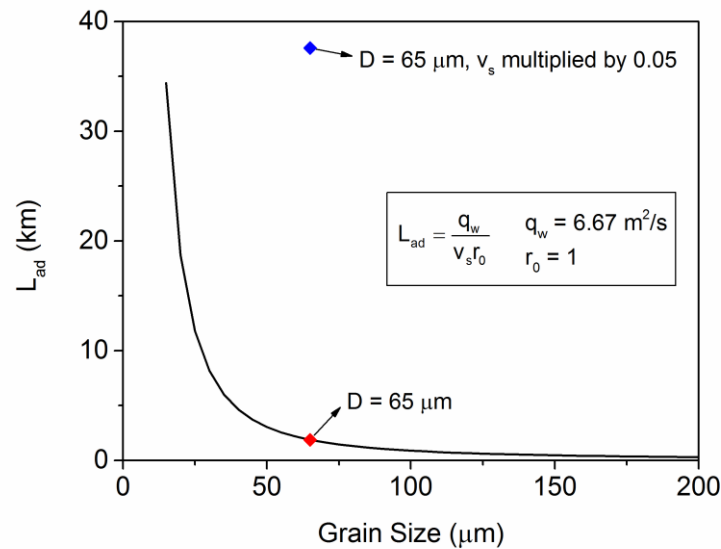
$$449 \quad q_s = q_{se} + (q_{sf} - q_{se}) e^{-\frac{x}{L_{ad}}} \quad (33)$$

450 Here q_{sf} is the sediment supply rate per unit width at the upstream end. According to Eq. (33), q_s adjusts exponentially in space
 451 from q_{sf} to q_{se} , which also coincides with our simulation in Section 3.1 as shown in Figs. 3-6. The adaptation length L_{ad} is the
 452 key parameter that controls the distance for q_s to approach the equilibrium sediment transport rate q_{se} . More specifically, q_s
 453 attains $1 - 1/e$ (i.e. 63.2%) of its adjustment from q_{sf} to q_{se} over a distance L_{ad} . Therefore, the larger the adaptation length, the
 454 slower q_s adjusts in space, so that the more evident lag effects and diffusivity are exhibited in the entrainment form. In the flux
 455 form, however, the sediment load responds simultaneously with the flow conditions, so that $L_{ad} = 0$ and $q_s = q_{se}$ along the
 456 entire channel reach.

457 For the case of uniform sediment in Section 3.1, $q_w = 6.67 \text{ m}^2/\text{s}$ and r_0 is specified as unity. Therefore, the value of
 458 L_{ad} is determined only by the sediment fall velocity v_s . Figure 9 shows the value of the adaptation length L_{ad} for various
 459 sediment grain sizes, with the sediment fall velocity v_s calculated by the relation of Dietrich (1982). From the figure we can



460 see that L_{ad} decreases sharply with the increase of grain size, indicating that the lag effects between sediment transport and
 461 flow conditions are evident for very fine sediment but gradually disappear when sediment is sufficiently coarse. For the
 462 sediment grain size of $65 \mu\text{m}$ implemented in Section 3.1, the corresponding $L_{ad} = 1.88 \text{ km}$, which is much smaller than the
 463 200 km reach of the computational domain. Therefore, the predictions of the flux form and the entrainment form show little
 464 difference. However, if we arbitrarily multiply the sediment fall velocity by a factor of 0.05 , then L_{ad} becomes 37.60 km . With
 465 such a large adaptation length, it is no surprise that the entrainment form gives very different prediction from the flux form.



466 **Figure 9.** Relation between adaptation length L_{ad} and grain size D . The values of flow discharge per unit width q_w and recovery
 467 coefficient r_0 are the same as those in Section 3.1. The relation of Dietrich (1982) is implemented for sediment fall velocity.
 468

469 The evolution of bed elevation z_b can also be affected by the value of L_{ad} . For example in the case of uniform sediment
 470 in Section 3.1, the flux form corresponds to an adaption length of zero. As a result, the flux form yields a spatial derivative of
 471 q_s near the upstream end that is relatively large, thus leading to fast degradation from the upstream end. In the case of the
 472 entrainment form, however, the spatial derivative of q_s is small with a large L_{ad} , thus leading to a slower and more diffusive
 473 bed degradation. This is especially evident when we arbitrarily reduce the sediment fall velocity by a factor of 0.05 , while
 474 keeping grain size invariant.

475 The above analysis also holds for sediment mixtures, except that each grain size range will have its own adaptation
 476 length. Here we neglect the temporal derivative in Eq. (29) and analyze only the spatial adjustment of sediment load. If we
 477 neglect the spatial derivative in Eq. (29) and conduct a similar analysis for sediment concentration, we would find that the
 478 temporal adjustment of sediment concentration is also described by an exponential function of time, in analogy to Eq. (33).



479 **4.2 Patterns of grain sorting: advection vs. diffusion**

480 In Section 3.2 we find that the flux form and entrainment form of the Exner equation provide very different patterns
 481 of grain sorting for sediment mixtures: kinematic sorting waves are evident in the flux form but are diffused out in the
 482 entrainment form. The diffusivity of grain sorting becomes smaller and the kinematic waves appear, however, if we arbitrarily
 483 increase the sediment fall velocity by a factor of 20. In this section, we explain this behavior by analyzing the governing
 484 equations.

485 First we rewrite the sediment transport relation of Naito et al. (accepted subject to revision) in the following form,

486
$$q_{sei} = F_i q_{ri} \quad (34)$$

487
$$q_{ri} = \frac{u_*^3}{RgC_f} A_i \left(\tau_g^* \frac{D_g}{D_i} \right)^{B_i} \quad (35)$$

488 Substituting Eq. (34) into Eq. (6), which is the governing equation for surface fraction F_i in the flux form, we get

489
$$\frac{1}{I_f} (1 - \lambda_p) \left[L_a \frac{\partial F_i}{\partial t} + (F_i - f_{li}) \frac{\partial L_a}{\partial t} \right] = f_{li} \frac{\partial \sum_{j=1}^n F_j q_{rj}}{\partial x} - \frac{\partial F_i q_{ri}}{\partial x} \quad (36)$$

490 Equation (36) can be written in the form of a kinematic wave equation with source terms as below,

491
$$\frac{\partial F_i}{\partial t} + c_{Fi} \frac{\partial F_i}{\partial x} = SF_i \quad (37)$$

492
$$c_{Fi} = \frac{I_f q_{ri}}{(1 - \lambda_p) L_a} (1 - f_{li}) \quad (38)$$

493
$$SF_i = - \frac{I_f F_i (1 - f_{li})}{(1 - \lambda_p) L_a} \frac{\partial q_{ri}}{\partial x} + \frac{I_f f_{li}}{(1 - \lambda_p) L_a} \frac{\partial \sum_{j=1}^{n, j \neq i} F_j q_{rj}}{\partial x} - \frac{F_i - f_{li}}{1 - \lambda_p} \frac{\partial L_a}{\partial t} \quad (39)$$

494 where c_{Fi} is the i -th celerity of kinematic wave and SF_i denotes source terms. Since the surface geometric mean grain size D_{sg} ,
 495 the total sediment load per unit width q_{sT} (which equals the equilibrium sediment transport rate q_{sET}), and the geometric mean
 496 grain size of sediment load D_{lg} are all closely related to the surface grain size fractions F_i , the evolution of these three



497 parameters exhibit marked advective behavior when simulated by the flux form of the Exner equation. However, the evolution
 498 of bed elevation z_b is related with $\partial q_{sT}/\partial x$, which is dominated by diffusion if q_{sT} is predominantly slope-dependent.

499 Now we turn to the entrainment form of the Exner equation. Combined with the sediment transport rate per unit width
 500 $q_{si} = huC_i = q_w C_i$ and the dimensionless entrainment rate $E_i = r_{0i} q_{sei}/q_w$, Eq. (16) and Eq. (15) can be written as,

$$501 \quad \frac{1}{I_f} \frac{\partial \left(\frac{q_{si}}{u} \right)}{\partial t} + \frac{\partial q_{si}}{\partial x} = \frac{v_{si} r_{0i}}{q_w} (q_{sei} - q_{si}) \quad (40)$$

$$502 \quad \frac{1}{I_f} (1 - \lambda_p) \left[L_a \frac{\partial F_i}{\partial t} + (F_i - f_{li}) \frac{\partial L_a}{\partial t} \right] = f_{li} \sum_{j=1}^n \frac{v_{sj} r_{0j}}{q_w} (q_{sej} - q_{sj}) - \frac{v_{si} r_{0i}}{q_w} (q_{sei} - q_{si}) \quad (41)$$

503 where Eq. (40) denotes the conservation of suspended sediment and Eq. (41) denotes the conservation of bed material. If we
 504 rewrite Eq. (40) in the following form,

$$505 \quad q_{si} = q_{sei} - \frac{q_w}{v_{si} r_{0i}} \left[\frac{1}{I_f} \frac{\partial \left(\frac{q_{si}}{u} \right)}{\partial t} + \frac{\partial q_{si}}{\partial x} \right] \quad (42)$$

506 then q_{si} can be solved iteratively. With an initial guess of $q_{si} = q_{sei}$ and neglecting the temporal derivatives, we obtain the second
 507 order solution of q_{si} as,

$$508 \quad q_{si} = q_{sei} - \frac{q_w}{v_{si} r_{0i}} \frac{\partial}{\partial x} \left(q_{sei} - \frac{q_w}{v_{si} r_{0i}} \frac{\partial q_{sei}}{\partial x} \right) \quad (43)$$

509 Details of the iteration are given in Appendix B.

510 Substituting Eq. (43) and Eq. (34) into Eq. (41), we find that

$$511 \quad \frac{1}{I_f} (1 - \lambda_p) \left[L_a \frac{\partial F_i}{\partial t} + (F_i - f_{li}) \frac{\partial L_a}{\partial t} \right] = f_{li} \sum_{j=1}^n \frac{\partial}{\partial x} \left(F_j q_{rj} - \frac{q_w}{v_{sj} r_{0j}} \frac{\partial F_j q_{rj}}{\partial x} \right) - \frac{\partial}{\partial x} \left(F_i q_{ri} - \frac{q_w}{v_{si} r_{0i}} \frac{\partial F_i q_{ri}}{\partial x} \right) \quad (44)$$

512 Expanding out the last two terms in Eq. (44) using the chain rule, after some work the relation for the conservation of bed
 513 material can be expressed as,



$$514 \quad \frac{\partial F_i}{\partial t} + c_{Ei} \frac{\partial F_i}{\partial x} - \nu_i \frac{\partial^2 F_i}{\partial x^2} = SE_i \quad (45)$$

$$515 \quad c_{Ei} = \frac{(1 - f_{li}) I_f}{(1 - \lambda_p) L_a} \left(q_{ri} - 2 \frac{q_w}{\nu_{si} r_{oi}} \frac{\partial q_{ri}}{\partial x} \right) \quad (46)$$

$$516 \quad \nu_i = \frac{(1 - f_{li}) I_f q_w q_{ri}}{(1 - \lambda_p) L_a \nu_{si} r_{oi}} \quad (47)$$

$$517 \quad SE_i = \frac{I_f f_{li}}{(1 - \lambda_p) L_a} \sum_{j=1}^{n, j \neq i} \frac{\partial}{\partial x} \left(F_j q_{rj} - \frac{q_w}{\nu_{sj} r_{oj}} \frac{\partial F_j q_{rj}}{\partial x} \right) - \frac{(1 - f_{li}) I_f}{(1 - \lambda_p) L_a} \left(F_i \frac{\partial q_{ri}}{\partial x} - \frac{q_w}{\nu_{si} r_{oi}} F_i \frac{\partial^2 q_{ri}}{\partial x^2} \right) - \frac{F_i - f_{li}}{L_a} \frac{\partial L_a}{\partial t} \quad (48)$$

518 where c_{Ei} is the celerity of kinematic wave, ν_i is the diffusivity coefficient, and SE_i denote source terms.

519 From Eq. (45) we can see that the governing equation for F_i in the entrainment form is an advection-diffusion equation,
 520 rather than the kinematic wave equation of the flux form. The surface geometric mean grain size D_{sg} is governed by Eq. (45),
 521 with describes the variation of the surface fractions F_i from which it is computed. The equilibrium sediment transport rate q_{sei}
 522 is governed by Eq. (45) because we implement a surface-based sediment transport relation as shown in Eq. (34). According to
 523 Eq. (43), the total sediment load per unit width q_{st} and the geometric mean grain size of sediment load D_{lg} must also be closely
 524 related to the surface grain size fractions F_i . Therefore, the diffusion terms in Eq. (45) can lead to the dissipation of the
 525 kinematic waves in Figs. 7(b), 7(c), and 7(d).

526 From Eq. (47), we can also see that the diffusivity coefficient ν_i is related to the sediment fall velocity ν_{si} : the larger
 527 the sediment fall velocity, the smaller the diffusivity coefficient. Thus when we increase the sediment fall velocity arbitrarily
 528 by a factor of 20 in Section 3.2, the kinematic waves become more evident as a result of the reduction of diffusivity.

529 Moreover if we compare the celerity of kinematic waves in both the flux form and the entrainment form, we have

$$530 \quad \frac{c_{Ei}}{c_{Fi}} = 1 - r_{ci} \quad (49)$$

$$531 \quad r_{ci} = 2 \frac{L_{adi}}{q_{ri}} \frac{\partial q_{ri}}{\partial x} \quad (50)$$

532 where L_{adi} is the adaptation length for the i -th size range as defined by Eq. (31). More specifically, the value of r_{ci} depends on
 533 $\partial q_{ri} / \partial x$. For our numerical simulation in Section 3.2, $\partial q_{ri} / \partial x > 0$ as a result of bed degradation progressing from the upstream
 534 end, thus leading to a positive value of r_{ci} and an entrainment celerity c_{Ei} that is smaller than the corresponding flux celerity



535 c_{Fi} . This is consistent with our numerical results: the kinematic waves in Fig. 8 predicted by the entrainment form are somewhat
 536 smaller than the kinematic waves in Fig. 6 predicted by the flux form.

537 4.3 Modeling implications and limitations

538 In Section 3, two numerical cases are conducted to compare the flux form and the entrainment form of the Exner
 539 equation, but only within 0.2 year after the cutoff of sediment supply. Here we run both numerical cases for a longer time (5
 540 years). Table 4 shows the results of the case of uniform sediment (as described in Section 3.1) within 5 years, and Table 5
 541 shows the results of the case of sediment mixtures (as described in Section 3.2) within 5 years. For both cases, the δ values,
 542 corresponding to relative deviation between the flux and entrainment forms, become quite small after 1 year, thus validating
 543 our assumption that the predictions of the two forms tend to be most evident shortly after disruption, but gradually diminish
 544 over a longer time scale. Moreover, if the water and sediment supply are kept constant for a sufficiently long time, the flux
 545 form and entrainment form of Exner equation predict exactly the same equilibrium, under which the equilibrium sediment
 546 transport rate (of each size range) equals to the sediment supply rate (of each size range).

547 **Table 4.** Quantification of the difference between predictions of the flux form and the entrainment form in the case of uniform
 548 sediment. The maximum δ in the calculational domain are presented for each of 5 years.

		1 yr	2 yr	3 yr	4 yr	5 yr
original v_s	$\delta(z_b)$	2.97 %	2.67 %	2.56 %	2.54 %	2.55 %
	$\delta(q_s)$	2.97 %	1.77 %	1.31 %	1.09 %	1.00 %

549

550 **Table 5.** Quantification of the difference between predictions of the flux form and the entrainment form in the case of sediment
 551 mixtures. The maximum δ in the calculational domain are presented for each of five years.

		1 yr	2 yr	3 yr	4 yr	5 yr
original v_s	$\delta(z_b)$	2.16 %	1.85 %	1.74 %	1.70 %	1.71 %
	$\delta(q_{sT})$	2.90 %	1.84 %	1.51 %	1.40 %	3.89 %
	$\delta(D_{sg})$	5.22 %	3.93 %	3.54 %	4.74 %	3.92 %
	$\delta(D_{lg})$	0.76 %	0.61 %	0.96 %	1.34 %	0.82 %

552

553 Based on the numerical modeling and mathematical analysis in this paper, we summarize below the circumstances
 554 under which the entrainment form of the Exner equation might be required. (1) The difference in the predictions of the two
 555 forms of the Exner equation tends to be large shortly after disruption, but gradually diminishes over time. Therefore, we suggest
 556 that the entrainment form of Exner equation should be used at short time scale (e.g., within a flood event), but that the flux
 557 form of Exner equation is applicable to long-term river morphodynamics (e.g., more than one year). (2) The entrainment form
 558 of the Exner equation is necessary if sorting processes are to be studied. The flux form of Exner equation cannot consider the



559 lag effects and diffusivity of individual size fractions, and therefore will result in an overestimation of the effect of advection
560 on sorting processes. (3) The entrainment form of the Exner equation is necessary when dealing with fine-grained sediment
561 (or more specifically sediment with small fall velocity), since the adaptation length L_a and the diffusivity coefficient v_i are
562 large under such circumstances. The flux form of the Exner equation is particularly applicable for coarse sediment, or when
563 the sediment transport is dominated by bedload (e.g. gravel-bed rivers). The above results could have practical implications in
564 regard to a wide range of issues including dam construction, water and sediment regulation, flood management, and ecological
565 restoration schemes. The results can also be used as a reference for other fine grained fluvial systems similar to the LYR, such
566 as the Pilcomayo River in Paraguay/Argentina, South America (Martín-Vide et al., 2014).

567 It should be noted that in the morphodynamic models of this paper, we implement the mass and momentum
568 conservation equations for clear water (i.e., Eq. (1) and Eq. (2)) to calculate flow hydraulics, instead of the mass and momentum
569 equations for water-sediment mixture as suggested by Cao et al. (2004) and Cao et al. (2006). More specifically, Cui et al.
570 (2005) have pointed out that when sediment concentration in the water is sufficiently small, bed elevation can be taken to be
571 unchanging over characteristic hydraulic time scales, and the effects of flow-bed exchange on flow hydraulics can be neglected.
572 For the two simulation cases in this paper, the volume sediment concentration C drops from about 2×10^{-3} to about 2×10^{-4} in
573 the case of uniform sediment, and from about 4×10^{-3} to about 4×10^{-4} in the case of sediment mixtures, due to the cutoff of
574 sediment supply at the upstream end. These dilute concentrations validate our implementation of mass and momentum
575 conservation equations for clear water. Our assumption is not necessarily correct for the entire Yellow River. Upstream of our
576 study reach, and especially upstream of Sanmenxia Dam, the flow is often hyperconcentrated (Xu, 1999).

577 Considering the fact that in our numerical simulations a constant inflow discharge (along with a flood intermittency
578 factor) is implemented, and also considering that the morphodynamic time scale is much larger than the hydraulic time scale
579 in our case, the quasi-steady approximation or even the normal flow approximation can be introduced to further save
580 computational efforts (Parker, 2004). But one thing that should be noted is that in our simulation results in Section 3, the bed
581 exhibits an inverse slope near the upstream end. The normal flow assumption becomes invalid under such circumstances, so
582 requiring a full unsteady shallow water model.

583 By definition, the recovery coefficient r_0 is the ratio of the near-bed to the flux-depth-averaged concentration of
584 suspended load, and is thus related to the concentration profile. In our simulation r_0 is specified as unity. That is, density
585 stratification effects of suspended sediment are neglected, and the vertical profile of sediment concentration is regarded as
586 uniform. However in natural rivers, the value of r_0 can vary significantly under different circumstances (Cao et al., 2004; Duan
587 and Nanda, 2006; Zhang and Duan, 2011; Zhang et al., 2013). In general, the value of r_0 is no less than unity and can be as
588 large as 12 (Zhang and Duan, 2011). Therefore according to our mathematical analysis in Section 4.1 and 4.2, $r_0 = 1$
589 corresponds to a maximum adaptation length L_{ad} , a maximum diffusivity coefficient v_i , and a minimum ratio of celerities c_{Ei}/c_{Fi} ,
590 thus leading to the largest difference between the flux form and the entrainment form. When sediment concentration is
591 sufficiently high, hindered settling effects reduce the sediment fall velocity. Considering the fact that the sediment



592 concentrations considered in our simulation are fairly small, hindered effects are not likely significant. More study on
593 stratification and hindered settling effects are merited in the case of the LYR.

594 **5 Conclusion**

595 In this paper, we compare two formulations for sediment mass conservation in context of the Lower Yellow River,
596 i.e. the flux form of Exner equation and the entrainment form of Exner equation. In the flux form of the Exner equation, the
597 conservation of bed material is related to the streamwise gradient of sediment transport rate, which is in turn computed based
598 on the quasi-equilibrium assumption according to which the local sediment transport rate equals the capacity rate. In the
599 entrainment form of the Exner equation, on the other hand, the conservation of bed material is related to the difference between
600 the entrainment rate of sediment from the bed into the flow and the deposition rate of sediment from the flow onto the bed. A
601 nonequilibrium sediment transport formulation is applied, so that the sediment transport rate can lag in space and time behind
602 changing flow conditions. Despite the fact that the entrainment form is usually recommended for the morphodynamic modeling
603 of the LYR due to its fine-grained sediment, there has been little discussion of the differences in predictions between the two
604 forms.

605 Here we implement a 1-D morphodynamic model for this problem. The fully unsteady Saint Venant Equations are
606 implemented for the hydraulic calculation. Both the flux form and the entrainment form of Exner equation are implemented
607 for sediment conservation. For each formulation, we include the options of both uniform sediment and sediment mixtures.
608 Two generalized versions of the Engelund-Hansen relation specifically designed for the LYR are implemented to calculate the
609 quasi-equilibrium sediment transport rate (i.e., sediment transport capacity). They are the version of Ma et al. (2017) for
610 uniform sediment, and the version of Naito et al. (accepted subject to revision) for sediment mixtures. The method of Viparelli
611 et al. (2010) is implemented to store and access bed stratigraphy as the bed aggrades and degrades. We apply the
612 morphodynamic model to two cases with conditions typical of the LYR.

613 In the first case, a uniform bed material grain size of 65 μm is implemented. We study the effect of cutoff of sediment
614 supply, as occurred after the operation of Xiaolangdi Dam in 1999. We find that the flux form and the entrainment form give
615 very similar predictions for this case. Through quantification of the difference between the two forms with a normalized
616 measure of relative difference, we find that difference in the prediction of bed elevation is quite small ($< 4\%$), but difference
617 in the prediction of sediment load can be relatively large (about 20%) shortly after the cutoff of sediment supply. Moreover,
618 the predictions of the entrainment form become very different from those of the flux form if we arbitrarily reduce the sediment
619 fall velocity by a multiplicative factor of 0.05, while keeping grain size unchanged.

620 The results for the case of uniform sediment can be explained by analyzing the governing equation of sediment load
621 q_s . In the flux form, the volume sediment transport rate per unit width q_s = the local equilibrium (capacity) value q_{se} . But in
622 the entrainment form, we find that the difference between q_s and q_{se} decays exponentially in space. The adaptation length L_{ad}
623 = $q_w / (v_s r_0)$ is the key parameter that controls the distance for q_s to approach its equilibrium value q_{se} . The larger the adaptation



624 length, the more different the predictions of the two forms will be. For computational conditions in this case, the adaption
625 length is relatively small ($L_{ad} = 1.88$ km), but it becomes much larger ($L_{ad} = 37.6$ km) if sediment fall velocity is arbitrarily
626 divided by a factor of 20.

627 In the second case the bed material consists of mixtures ranging from $15 \mu\text{m}$ to $500 \mu\text{m}$. We find that the flux form
628 and the entrainment form give very different patterns of grain sorting. Evident kinematic waves occur at various timescales in
629 the flux form, but no evident kinematic waves can be observed in the entrainment form. The different sorting patterns are
630 reflected in the evolution of surface geometric mean grain size D_{sg} , total sediment load q_{ST} and geometric mean grain size of
631 sediment load D_{lg} , but are not reflected in the evolution of bed elevation z_b . Kinematic waves appear in the entrainment form
632 if we arbitrarily increase the sediment fall velocity by multiplying a factor of 20 without changing the grain size. This large
633 increase in fall velocity leads to a large decrease in adaptation length, so that the entrainment form behaves much more like
634 the flux form. This notwithstanding, the kinematic waves are still more diffusive and slower than those predicted by the flux
635 form.

636 The different sorting patterns exhibited in the case of sediment mixtures can be explained by analyzing the governing
637 equation for bed surface fractions F_i , i.e. the grain size-specific conservation of bed material. We find that in the flux form, the
638 governing equation for F_i can be written in the form of a kinematic wave equation. In the entrainment form, however, the
639 governing equation for F_i is an advection-diffusion equation. It is the diffusion term which can lead to the dissipation of
640 kinematic waves. Moreover, in the advection-diffusion equation arising from the entrainment form, the coefficient of
641 diffusivity is inversely proportional to the sediment fall velocity. In addition, under the condition of bed degradation the wave
642 celerity is smaller than the celerity arising from the flux form.

643 Overall, our results indicate that the more complex entrainment form of the Exner equation might be required under
644 the following circumstances: (1) when short-term (e.g., within a flood event) river morphodynamics is considered; (2) when
645 sorting processes are studied; and (3) when fine-grained sediment (or more specifically sediment with small fall velocity) is
646 considered.

647 **Appendix A: Comparison of two relations for sediment fall velocity: Dietrich (1982) against Ferguson and Church** 648 **(2004)**

649 In this paper, we implement the relation of Dietrich (1982) to calculate sediment fall velocity v_s . The relation is,

$$650 \quad v_s = R_f \sqrt{RgD} \quad (\text{A1})$$

$$651 \quad \ln(R_f) = -b_1 + b_2 \ln(\text{Re}_p) - b_3 [\ln(\text{Re}_p)]^2 - b_4 [\ln(\text{Re}_p)]^3 + b_5 [\ln(\text{Re}_p)]^4 \quad (\text{A2})$$



652
$$\text{Re}_p = \frac{\sqrt{RgDD}}{\nu} \quad (\text{A3})$$

653 where $b_1 = 2.891394$, $b_2 = 0.95296$, $b_3 = 0.056835$, $b_4 = 0.002892$, $b_5 = 0.000245$, and $\nu = 10^{-6}$ is the kinematic viscosity of
654 water.

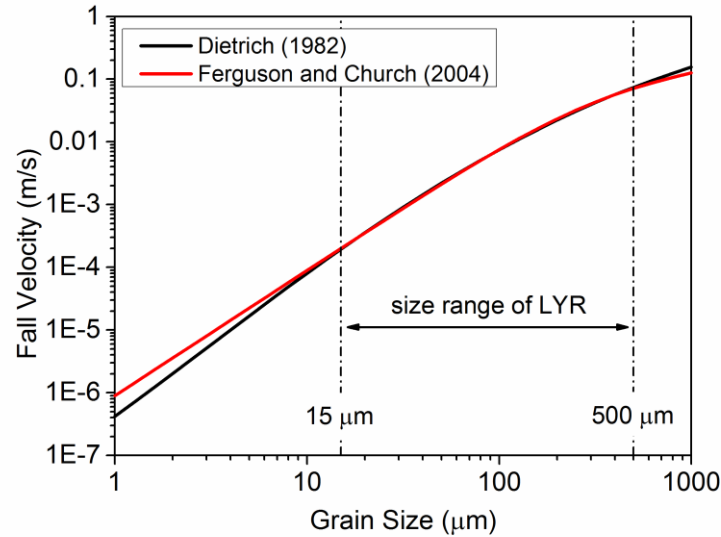
655 Another widely used relation for sediment fall velocity is the relation of Ferguson and Church (2004), which is
656 regarded as applying to nearly the entire range of viscous to turbulent conditions.

657
$$v_s = \frac{RgD^2}{C_1\nu + (0.75C_2RgD^3)^{0.5}} \quad (\text{A4})$$

658 where $C_1 = 18$ and $C_2 = 0.4$ for smooth spheres; $C_1 = 18$ and $C_2 = 1.0$ for sieve diameters of natural sand; and $C_1 = 20$ and C_2
659 $= 1.1$ for nominal diameters of natural sand. More specifically, the relation of Ferguson and Church (2004) converges on
660 Stokes' law for small grains, and to a constant drag coefficient for large grains.

661 Considering the fact that the sediment of LYR is finer than most sand-bed rivers (Ma et al., 2017), here we compare
662 the two relations for sediment fall velocity in the context of the LYR. The two parameters in Ferguson and Church are specified
663 as $C_1 = 18$ and $C_2 = 1.0$. In our simulation, the sediment size range of the LYR is specified as $15 \mu\text{m} \sim 500 \mu\text{m}$.

664 According to Fig. A1, the relation of Dietrich (1982) and the relation of Ferguson and Church (2004) coincide with
665 each other within this size range, thus justifying our implementation of Dietrich (1982) in the simulation. For grain sizes
666 smaller than $15 \mu\text{m}$, sediment becomes washload in the LYR and Dietrich (1982) predicts sediment fall velocities that are
667 smaller than those predicted by Ferguson and Church (2004). For sediment coarser than $500 \mu\text{m}$, Dietrich (1982) somewhat
668 overestimates sediment fall velocity compared with Ferguson and Church (2004).



669
 670 **Figure A1.** Comparison of two relations for sediment fall velocity: Dietrich (1982) and Ferguson and Church (2004)

671 **Appendix B: Iterative solution of sediment transport rate q_{si} in the entrainment form**

672 The parameter q_{si} in Eq. (40) is solved iteratively as below,

673
$$q_{si}^{(m+1)} = q_{sei} - \frac{q_w}{v_{si} r_{oi}} \left[\frac{1}{I_f} \frac{\partial \left(\frac{q_{si}^{(m)}}{u} \right)}{\partial t} + \frac{\partial q_{si}^{(m)}}{\partial x} \right] \quad (\text{B1})$$

674 where the superscript denotes the order of iteration. The following zero-order solution is specified as an initial value;

675
$$q_{si}^{(0)} = q_{sei} \quad (\text{B2})$$

676 From this we can get the first order and the second order solution,

677
$$q_{si}^{(1)} = q_{sei} - \frac{q_w}{v_{si} r_{oi}} \left[\frac{1}{I_f} \frac{\partial \left(\frac{q_{sei}}{u} \right)}{\partial t} + \frac{\partial q_{sei}}{\partial x} \right] \quad (\text{B3})$$



$$q_{si}^{(2)} = q_{sei} - \frac{q_w}{v_{si}r_{oi}} \frac{1}{I_f} \frac{\partial}{\partial t} \frac{1}{u} \left\{ q_{sei} - \frac{q_w}{v_{si}r_{oi}} \left[\frac{1}{I_f} \frac{\partial \left(\frac{q_{sei}}{u} \right)}{\partial t} + \frac{\partial q_{sei}}{\partial x} \right] \right\} - \frac{q_w}{v_{si}r_{oi}} \frac{\partial}{\partial x} \left\{ q_{sei} - \frac{q_w}{v_{si}r_{oi}} \left[\frac{1}{I_f} \frac{\partial \left(\frac{q_{sei}}{u} \right)}{\partial t} + \frac{\partial q_{sei}}{\partial x} \right] \right\} \quad (B4)$$

The second order iterative solution in Eq. (B4) is tedious in form, but the only terms of importance on the right-hand side are the spatial derivatives. Therefore we drop the time derivatives for simplicity. This gives,

$$q_{si} = q_{sei} - \frac{q_w}{v_{si}r_{oi}} \frac{\partial}{\partial x} \left(q_{sei} - \frac{q_w}{v_{si}r_{oi}} \frac{\partial q_{sei}}{\partial x} \right) \quad (B5)$$

which corresponds to Eq. (41) as implemented in Section 4.2.

684 Notation

- 685 C depth-flux-averaged sediment concentration
- 686 C_f dimensionless bed resistance coefficient
- 687 C_z dimensionless Chezy resistance coefficient
- 688 c_b near-bed sediment concentration
- 689 c_E celerity of the kinematic wave corresponding to F_i in the entrainment form
- 690 c_{Fi} celerity of the kinematic wave corresponding to F_i in the flux form
- 691 D sediment grain size
- 692 E dimensionless entrainment rate of sediment
- 693 F_i volumetric fraction of surface material in the i -th size range
- 694 f_{li} volumetric fraction of sediment in the i -th size range exchanged across the surface-substrate interface
- 695 g gravitational acceleration
- 696 h water depth
- 697 I_f flood intermittency factor
- 698 L_a thickness of active layer
- 699 L_{ad} adaptation length of suspended load
- 700 p_{si} volumetric fraction of bed material load in the i -th size range
- 701 q_{ri} normalized sediment transport rate per unit width for the i -th size range, defined by Eq. (34)
- 702 q_s volumetric sediment transport rate per unit width



- 703 q_{se} equilibrium volumetric sediment transport rate (capacity) per unit width
704 q_{sf} sediment supply rate per unit width
705 q_w flow discharge per unit width
706 R submerged specific gravity of sediment
707 r_0 user-specified parameter denoting the ratio between the near-bed sediment concentration and the flux-averaged sediment
708 concentration
709 S bed slope
710 t time
711 u depth-averaged flow velocity
712 u_* shear velocity
713 v_s sediment fall velocity
714 x streamwise coordinate
715 z_b bed elevation
716 α coefficient in Eq. (6) for interfacial exchange fractions
717 Δt_h time step for hydraulic calculation
718 Δt_m time step for morphologic calculation
719 Δx spatial step length.
720 δ normalized parameter quantifying the fraction difference between the entrainment form and the flux form.
721 λ_p porosity of bed deposit
722 ν_i diffusivity coefficient corresponding to F_i in the entrainment form;
723 ρ density of water
724 ρ_s density of sediment
725 τ_b bed shear stress
726 τ^* dimensionless shear stress (Shields number)

727 **Competing interests**

728 The authors declare that they have no conflict of interest.

729 **Acknowledgments**

730 The participation of Chenge An and Xudong Fu was made possible in part by grants from the National Natural Science
731 Foundation of China (grants 51525901 and 91747207), and the Ministry of Science and Technology of China (grant
732 2016YFC0402406). The participation of Andrew J. Moodie, Hongbo Ma, Kensuke Naito, and Gary Parker were made possible



733 in part by grants from National Science Foundation (grant EAR-1427262). The participation of Yuanfeng Zhang was made
734 possible in part by grant from the National Natural Science Foundation of China (grant 51379087). Part of this research was
735 accomplished during Cheng An's visit in the University of Illinois at Urbana-Champaign, which was supported by the China
736 Scholarship Council (file no. 201506210320). The participation of Andrew J. Moodie was also supported by an National
737 Science Foundation Graduate Research Fellowship (grant 145068). We thank the Morphodynamics Class of 2016 at the
738 University of Illinois at Urbana-Champaign for their participation in preliminary modeling efforts.

739 **References**

- 740 An, C., Cui, Y., Fu, X., and Parker, G.: Gravel-bed river evolution in earthquake-prone regions subject to cycled hydrographs
741 and repeated sediment pulses, *Earth Surface Processes and Landforms*, 42, 2426-2438, doi:10.1002/esp.4195, 2017.
- 742 Armanini, A. and Di Silvio, G.: A one-dimensional model for the transport of a sediment mixture in non-equilibrium conditions,
743 *Journal of Hydraulic Research*, 26(3), 275-292, doi:10.1080/00221688809499212, 1988.
- 744 Bell, R. G. and Sutherland, A. J.: Nonequilibrium bedload transport by steady flows, *Journal of Hydraulic Engineering*, 109(3),
745 351-367, 1983.
- 746 Blom, A., Ribberink, J. S., and de Vriend, H. J.: Vertical sorting in bed forms: Flume experiments with a natural and a trimodal
747 sediment mixture, *Water Resources Research*, 39(2), 1025, doi:10.1029/2001WR001088, 2003.
- 748 Bohorquez, P. and Ancey, C.: Particle diffusion in non-equilibrium bedload transport simulations, *Applied Mathematical*
749 *Modeling*, 40(17-18), 7474-7492, doi:10.1016/j.apm.2016.03.044, 2016.
- 750 Bradley, B. R. and Venditti J G.: Reevaluating dune scaling relations, *Earth-Science Reviews*, 165, 356-376, 2017.
- 751 Brownlie, W. R.: Prediction of flow depth and sediment discharge in open channels, W. M. Keck Laboratory of Hydraulics
752 and Water Resources, California Institute of Technology, Pasadena, USA, Rep. KH-R-43A, 232 pp., 1981.
- 753 Cao, Z., Pender, G., Wallis, S., and Carling, P.: Computational dam-break hydraulics over erodible sediment bed, *Journal of*
754 *Hydraulic Engineering*, 130(7), 689-703, 2004.
- 755 Cao, Z., Pender, G., and Carling, P.: Shallow water hydrodynamic models for hyperconcentrated sediment-laden floods over
756 erodible bed, *Advances in Water Resources*, 29(4), 546-557, doi:10.1016/j.advwatres.2005.06.011, 2006.
- 757 Cui, Y., Parker, G., Lisle T. E., Pizzuto, J. E., and Dodd, A. M.: More on the evolution of bed material waves in alluvial rivers,
758 *Earth Surface Processes and Landforms*, 30, 107-114, doi:10.1002/esp.1156, 2005.
- 759 Dietrich, E. W.: Settling velocity of natural particles, *Water Resources Research*, 18(6), 1626-1982,
760 doi:10.1029/WR018i006p01615, 1982.
- 761 Dorrell, R. M. and Hogg, A. J.: Length and time scales of response of sediment suspensions to changing flow conditions,
762 *Journal of Hydraulic Engineering*, 138(5), 430-439, doi:10.1061/(ASCE)HY.1943-7900.0000532, 2012.
- 763 Duan, J. G. and Nanda, S. K.: Two-dimensional depth-averaged model simulation of suspended sediment concentration
764 distribution in a groyne field, *Journal of Hydrology*, 324(3-4), 426-437, 2006.



- 765 Einstein, H. A.: Bedload transport as a probability problem, PhD thesis, Mitt. Versuchsanst. Wasserbau Eidg. Tech. Hochsch,
766 Zurich, Switzerland, 1937.
- 767 El kadi Abderrezzak, K. and Paquier, A.: One-dimensional numerical modeling of sediment transport and bed deformation in
768 open channels, *Water Resources Research*, 45, W05404, doi:10.1029/2008WR007134, 2009.
- 769 Engelund, F. and Hansen, E.: A monograph on sediment transport in alluvial streams, Technisk Vorlag, Copenhagen, Denmark,
770 1967.
- 771 Exner, F. M.: Uber die Wechselwirkung zwischen Wasser und Geschiebe in Flussen, *Sitzber. Akad. Wiss Wien*, 134(2a), 169-
772 204, 1920, (in German).
- 773 Ferguson, R. I. and Church, M.: A simple universal equation for grain settling velocity, *Journal of Sedimentary Research*,
774 74(6), 933-937, doi:10.1306/051204740933, 2004.
- 775 Ganti, V., Lamb, M. P., and McElroy, B.: Quantitative bounds on morphodynamics and implications for reading the
776 sedimentary record, *Nature Communications*, 5, 3298, doi:10.1038/ncomms4298, 2014.
- 777 Guan, M., Wright, N. G., and Sleigh, P. A.: Multimode morphodynamic model for sediment-laden flows and geomorphic
778 impacts, *Journal of Hydraulic Engineering*, 141(6), doi:10.1061/(ASCE)HY.1943-7900.0000997, 2015
- 779 Guo, Q., Hu, C., and Takeuchi, K.: Numerical modeling of hyper-concentrated sediment transport in the lower Yellow River,
780 *Journal of Hydraulic Research*, 46(5), 659-667, doi:10.3826/jhr.2008.3009, 2008.
- 781 Harten, A., Lax, P. D., and van Leer, B.: On upstream differencing and Godunov-type schemes for hyperbolic conservation
782 laws, *SIAM Review*, 25(1), 35-61, 1983.
- 783 He, L., Duan, J. G., Wang G., and Fu, X.: Numerical simulation of unsteady hyperconcentrated sediment-laden flow in the
784 Yellow River, *Journal of Hydraulic Engineering*, 138(11), 958-969, doi:10.1061/(ASCE)HY.1943-7900.0000599,
785 2012.
- 786 Hirano, M.: On riverbed variation with armoring, *Proc. Jpn. Soc. Civ. Eng.*, 195, 55-65, 1971, (in Japanese).
- 787 Hoey, T. B. and Ferguson, R.: Numerical simulation of downstream fining by selective transport in gravel bed rivers: Model
788 development and illustration, *Water Resour. Res.*, 30(7), 2251–2260, doi:10.1029/94WR00556, 1994.
- 789 Ma, H., Nittrouer, J. A., Naito, K., Fu, X., Zhang, Y., Moodie A. J., Wang, Y., Wu, B., and Parker, G.: The exceptional
790 sediment load of fine-grained dispersal systems: Example of the Yellow River, China, *Science Advances*, 3(5),
791 e1603114, doi:10.1126/sciadv.1603114, 2017.
- 792 Mart ín-Vide, J. P., Amarilla, M., and Z árate, F. J.: Collapse of the Pilcomayo River, *Geomorphology*, 205(15), 155-163, 2014.
- 793 Meyer-Peter, E. and Müller, R.: Formulas for bed-load transport, in *Proceeding of the 2nd IAHR Meeting, International
794 Association for Hydraulic Research*, 7-9 June 1948, Stockholm, Sweden, 39-64, 1948.
- 795 Milliman, J. D. and Meade, R. H.: World-wide delivery of river sediment to the oceans, *The Journal of Geology*, 91(1), 1-21,
796 1983.
- 797 Minh Duc, B. and Rodi, W.: Numerical simulation of contraction scour in an open laboratory channel, *Journal of Hydraulic
798 Engineering*, 134(4), 367-377, doi:10.1061/(ASCE)0733-9429(2008)134:4(367), 2008.



- 799 Naito, K., Ma, H., Nittrouer, J., Zhang, Y., Wu, B., Wang, Y., and Parker, G.: Extended Engelund-Hansen type sediment
800 transport relation for mixtures based on the sand-silt-bed Lower Yellow River, China, *Journal of Hydraulic Research*,
801 accepted subject to revision, 2018.
- 802 National Research Council.: *River Science at the U.S. Geological Survey*. Washington, DC: The National Academies Press,
803 available at: <https://doi.org/10.17226/11773>, 2007.
- 804 Ni, J. R., Zhang, H. W., Xue, A., Wieprecht, S., and Borthwick, A. G. L.: Modeling of hyperconcentrated sediment-laden
805 floods in Lower Yellow River, *Journal of Hydraulic Engineering*, 130(10), 1025-1032, 2004.
- 806 Paola, C., Heller, P. L., and Angevine, C. L.: The large-scale dynamics of grain-size variation in alluvial basins, I: Theory,
807 *Basin Research*, 4, 73-90, 1992.
- 808 Parker, G.: *1D Sediment Transport Morphodynamics with Applications to Rivers and Turbidity Currents*, available at:
809 http://hydrolab.illinois.edu/people/parkerg/morphodynamics_e-book.htm, 2004.
- 810 Parker, G., Paola, C., and Leclair, S.: Probabilistic Exner sediment continuity equation for mixtures with no active layer,
811 *Journal of Hydraulic Engineering*, 126(11), 818-826, 2000.
- 812 Phillips, B. C. and Sutherland A. J.: Spatial lag effects in bedload sediment transport, *Journal of Hydraulic Research*, 27(1),
813 115-133, doi:10.1080/00221688909499247, 1989.
- 814 Toro, E. F.: *Shock-capturing methods for free-surface shallow flows*, John Wiley, 2001
- 815 Toro-Escobar, C. M., Parker, G., and Paola, C.: Transfer function for the deposition of poorly sorted gravel in response to
816 streambed aggradation, *Journal of Hydraulic Research*, 34(1), 35-53, doi:10.1080/00221689609498763, 1996.
- 817 Tsujimoto, T.: A probabilistic model of sediment transport processes and its application for erodible-bed problems, Ph.D.
818 thesis, Kyoto University, Kyoto, Japan, 1978, (in Japanese).
- 819 Viparelli, E., Sequeiros, O. E., Cantelli, A., Wilcock, P. R., and Parker, G.: River morphodynamics with creation/consumption
820 of grain size stratigraphy 2: numerical model, *Journal of Hydraulic Research*, 48(6), 727-741,
821 doi:10.1080/00221686.2010.526759, 2010.
- 822 Wang, S., Fu, B., Piao, S., Lü Y., Ciais, P., Feng, X., and Wang, Y.: Reduced sediment transport in the Yellow River due to
823 anthropogenic changes, *Nature Geoscience*, 9, 38-41, doi:10.1038/ngeo2602, 2016.
- 824 Wu, W. and Wang, S. S. Y.: One-dimensional modeling of dam-break flow over movable beds. *Journal of Hydraulic*
825 *Engineering*, 133(1), 48-58, 2007.
- 826 Wu, W. and Wang, S. S. Y.: One-dimensional explicit finite-volume model for sediment transport, *Journal of Hydraulic*
827 *Research*, 46(1), 87-98, 2008.
- 828 Wu, W., Vieira, D. A., and Wang, S. S. Y.: A 1-D numerical model for nonuniform sediment transport under unsteady flows
829 in channel networks, *Journal of Hydraulic Engineering*, 130(9), 914-923, doi:10.1061/(ASCE)0733-
830 9429(2004)130:9(914), 2004.
- 831 Xu, J.: Erosion caused by hyperconcentrated flow on the Loess Plateau of China, *Catena*, 36(1999), 1-19, 1999.



- 832 Zhang, H., Huang, Y., and Zhao, L: A mathematical model for unsteady sediment transport in the Lower Yellow River,
833 International Journal of Sediment Research, 16(2), 150-158, 2001.
- 834 Zhang, S. and Duan, J. G.: 1D finite volume model of unsteady flow over mobile bed, Journal of Hydrology, 405, 57-68,
835 doi:10.1016/j.jhydrol.2011.05.010, 2011.
- 836 Zhang, S., Duan, J. G., and Strelkoff T. S.: Grain-scale nonequilibrium sediment-transport model for unsteady flow, Journal
837 of Hydraulic Engineering, 139(1), 22-36, doi:10.1061/(ASCE)HY.1943-7900.0000645, 2013.